AFTAC

Air Force Technical Applications Center
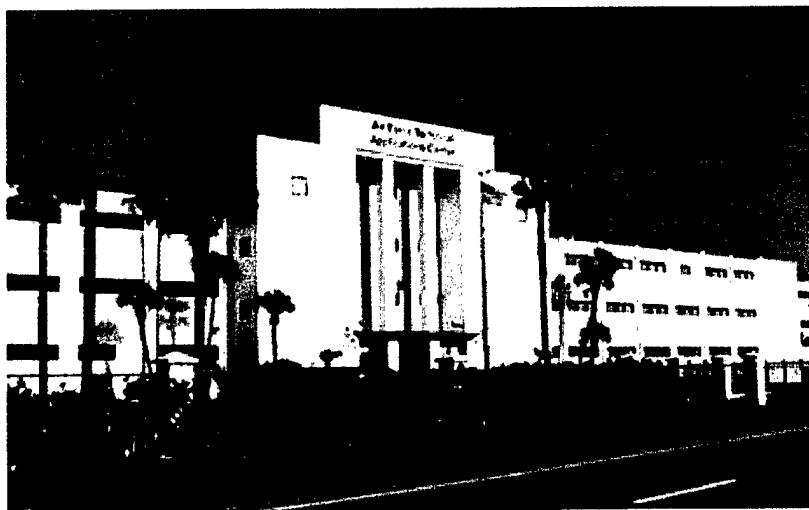
Directorate of Nuclear Treaty Monitoring

Detection and Azimuth Estimation by Infrasonic Arrays as a Function of Array Aperture and Signal Coherence

Robert R. Blandford

4 April 2002
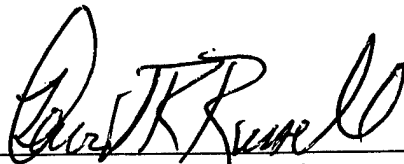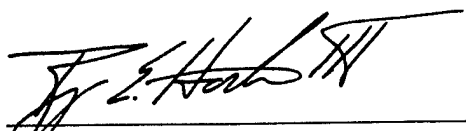
20031217 223

Report AFTAC-TR-02-005 has been reviewed and is approved for publication.

DAVID R, RUSSELL, SES
Director, Nuclear Treaty Monitoring

ROY E. HORTON III, Colonel, USAF
Commander

The overall classification of this report is UNCLASSIFIED

REPORT DOCUMENTATION PAGE		*Form Approved* *OMB No. 0704-0188*

Public reporting burden for this collection of information is estimated to average 1 hour per response, including the time for reviewing instructions, searching existing data sources, gathering and maintaining the data needed, and completing and reviewing this collection of information. Send comments regarding this burden estimate or any other aspect of this collection of information, including suggestions for reducing this burden to Department of Defense, Washington Headquarters Services, Directorate for Information Operations and Reports (0704-0188), 1215 Jefferson Davis Highway, Suite 1204, Arlington, VA 22202-4302. Respondents should be aware that notwithstanding any other provision of law, no person shall be subject to any penalty for failing to comply with a collection of information if it does not display a currently valid OMB control number. **PLEASE DO NOT RETURN YOUR FORM TO THE ABOVE ADDRESS.**

1. REPORT DATE *(DD-MM-YYYY)* 2 April 2002	2. REPORT TYPE Technical	3. DATES COVERED *(From - To)*

4. TITLE AND SUBTITLE Detection and Azimuth Estimation by Infrasonic Arrays as a Function of Array Aperture and Signal Coherence	5a. CONTRACT NUMBER
	5b. GRANT NUMBER
	5c. PROGRAM ELEMENT NUMBER
6. AUTHORS Robert R. Blandford	5d. PROJECT NUMBER
	5e. TASK NUMBER
	5f. WORK UNIT NUMBER

7. PERFORMING ORGANIZATION NAME(S) AND ADDRESS(ES) Air Force Technical Applications Center (AFTAC/TT) 1030 S. Highway A1A Patrick AFB FL 32925-3002	8. PERFORMING ORGANIZATION REPORT NUMBER AFTAC-TR-02-005
9. SPONSORING/MONITORING AGENCY	10. SPONSOR/MONITOR'S ACRONYM(S)
	11. SPONSOR/MONITOR'S REPORT NUMBERS

12. DISTRIBUTION/AVAILABILITY STATEMENT

Approved for Public Release; Distribution Unlimited

13. SUPPLEMENTARY NOTES

14. ABSTRACT

The Infrasound Experts Group of the Geneva Conference on Disarmament Ad Hoc Committee on a Nuclear Test Ban has recommended an infrasound array design consisting of four elements, with three elements forming an equilateral triangle and the fourth at the center of the triangle. The Experts recommended that the sides of the triangle be in the range of 1 to 3 kilometers (km).

In this report, correlation as a function of period and sensor spacing, and signal-to-noise ratios (S/N) as a function of period are estimated from atmospheric data from nuclear explosions of 2.2 and 2.6 kilotons (kt) recorded at sensors with spacings near 1 km and at distances from the explosions of 700 km. The correlation estimates are found to be consistent with parameters describing the spread of the signal in wavenumber space as discussed by Blandford (1997). These parameters were first estimated by Mack and Flinn (1971) for events of much larger yield at larger distances, longer period, and greater inter-sensor spacings. Data at 10 km spacing from a 2.2 kt event at a distance of 2200 km is found to be consistent with the Mack and Flinn parameters.

(Continued on next page)

15. SUBJECT TERMS

16. SECURITY CLASSIFICATION OF:			17. LIMITATION OF ABSTRACT	18. NUMBER OF PAGES	19a. NAME OF RESPONSIBLE PERSON Robert R. Blandford
a. REPORT UNCLASSIFIED	b. ABSTRACT UNCLASSIFIED	c. THIS PAGE UNCLASSIFIED	UNCLASSIFIED	60	19b.TELEPHONE NUMBER *(include area code)* (703) 648-6789

Standard Form 298 (Rev 8-98)
Prescribed by ANSI Std. 239-18

Block 14 Con't:

The correlation and S/N estimates are used to show that, for most International Monitoring Community applications, the optimum period for detection and azimuth estimation is 1 second, and that the optimum array aperture is 1 km.

Preliminary analysis of a signal at the TXAR infrasonic array from a White Sands 10-ton chemical explosion at a distance of 450 km gives much higher signal correlations at 1 Hertz (Hz) and 1 km spacing, suggesting that one-hop signals have approximately 1/5 the dispersion in azimuth and velocity as do multi-hop signals. Thus, paradoxically, it may be that an array larger than 1 km may be optimum for events at distances <500 km, while being suboptimal for events at greater distances.

CONTENTS

LIST OF FIGURES

LIST OF TABLES

ABSTRACT

The Infrasound Experts Group of the Geneva Conference on Disarmament Ad Hoc Committee on a Nuclear Test Ban has recommended an infrasound array design consisting of four elements, with three elements forming an equilateral triangle and the fourth at the center of the triangle. The Experts recommended that the sides of the triangle be in the range of 1 to 3 kilometers (km).

In this report, correlation as a function of period and sensor spacing, and signal-to-noise ratios (S/N) as a function of period are estimated from atmospheric data from nuclear explosions of 2.2 and 2.6 kilotons (kt) recorded at sensors with spacings near 1 km and at distances from the explosions of 700 km. The correlation estimates are found to be consistent with parameters describing the spread of the signal in wavenumber space as discussed by Blandford (1997). These parameters were first estimated by Mack and Flinn (1971) for events of much larger yield at larger distances, longer period, and greater inter-sensor spacings. Data at 10 km spacing from a 2.2 kt event at a distance of 2200 km is found to be consistent with the Mack and Flinn parameters. The correlation and S/N estimates are used to show that, for most International Monitoring Community applications, the optimum period for detection and azimuth estimation is 1 second, and that the optimum array aperture is 1 km.

Preliminary analysis of a signal at the TXAR infrasonic array from a White Sands 10-ton chemical explosion at a distance of 450 km gives much higher signal correlations at 1 Hertz (Hz) and 1 km spacing, suggesting that one-hop signals have approximately 1/5 the dispersion in azimuth and velocity as do multi-hop signals. Thus, paradoxically, it may be that an array larger than 1 km may be optimum for events at distances <500 km, while being suboptimal for events at greater distances.

ACKNOWLEDGMENTS

(This page intentionally left blank.)

INTRODUCTION

In an earlier report on infrasound array design, Blandford (1997) used coherence functions determined by Mack and Flinn (1971) (hereafter referred to as MF) from infrasound wave data from one of China's megaton-range explosions recorded at the Montana Large Aperture Meteorological Array (LAMA). The coherence was determined using periods T ≥10 seconds (sec), and at sensor intervals of x ≥7 kilometers (km). Using these results, Blandford (1997) showed that for a "detection" beam root-mean-square (rms) signal-to-noise (S/N) amplitude ratio of 1.5 at the expected detection period of 5 seconds for a 1 kiloton (kt) explosion, a 1-km aperture array may be expected to have an azimuth estimation standard error smaller than the experimentally observed 1.8° true azimuthal error. Thus, it appeared that an array aperture larger than 1 km, which would likely entail increased logistic expenses, would not be necessary for adequate azimuth estimation capability.

In addition, it was shown, assuming the MF data parameterization could be used to extrapolate to 1-sec period, that for array apertures of 2-3 km, 1 Hertz (Hz) signals would be substantially uncorrelated so that array signal estimates at this period would be poor. This could be undesirable if 1 Hz data were to be used for discrimination between explosion signals and other signals. Thus, again, a 1-km aperture was indicated.

A weakness in the work of Blandford (1997) was that there were no data to show that the MF data could be reliably extrapolated to 1 Hz. Moreover, there were no data available on the variation of S/N as a function of period from sources of interest. There were, however, data cited to show that the peak in the signal spectrum from 1 kt events at 1000 km is near 5 sec period, but it is not necessarily the case that this is the same as the peak in S/N, which is the critical parameter for detection and azimuth estimation. In addition, for both detection and azimuth estimation, capability increases in proportion to the time-bandwidth product. Thus, optimum capability may occur at a frequency higher than that for which there is the highest S/N.

In this report, 0.5- to 10-sec signals from the 2.6 kt nuclear atmospheric test, Tanana, recorded by a 1-km aperture array on Palmyra Island are examined. Based on these and other similar data, we find that extrapolation of the MF functions is justified. Consequently, the interaction of observed S/N with array aperture implies that the best 1-kt explosion detection <u>and</u> azimuth estimation performance is at 1-sec period and at an aperture of 1 km.

Figure 1, from Blandford (1997), illustrates the squared coherence as a function of period and element spacing, both parallel and perpendicular to the wavefront calculated from equation (1).

$$\gamma^2 = \left| \frac{\sin(2\pi k_o x \sin\Delta\theta)}{2\pi k_o x \sin\Delta\theta} \right|^2 \cdot \left| \frac{\sin(2\pi\Delta ky)}{2\pi\Delta ky} \right|^2 \tag{1}$$

In equation (1) γ is coherence, k_o is the wavenumber, $\Delta\theta$ is the spread in azimuth of the signal packet, Δk is the spread in wavenumber, and x and y are the relative locations of the two sensors.

Infrasound Squared Coherence, Parallel ...... and Perpendicular ____
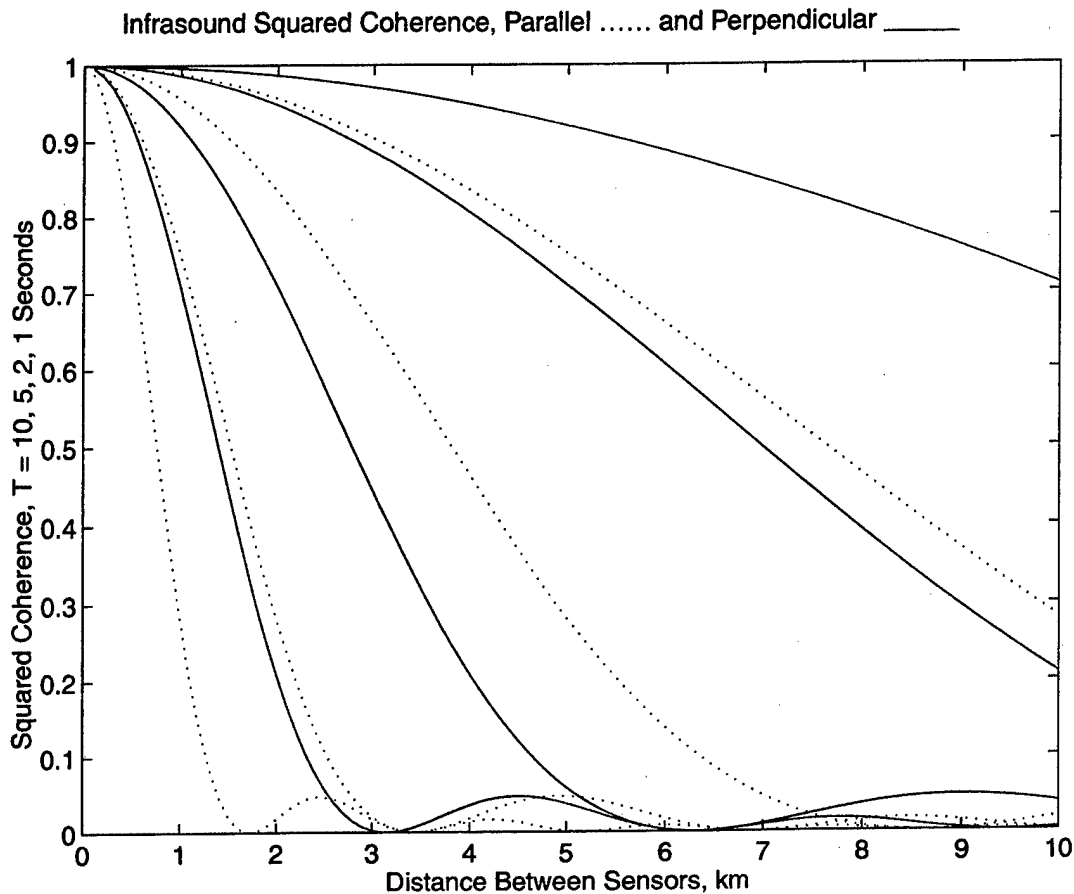
Figure 1. Squared coherence as a function of intersensor distance for T=10, 5, 2, and 1 seconds according to the equation above, using Δc=0.015 km/sec and ΔΘ=5° as determined from Mack and Flinn (1971), parallel and perpendicular to the wavefront. Observed correlation estimates should be compared to the theoretical estimates of coherence and not to squared coherence.

In subsequent sections, we discuss the Palmyra data, present the methods used to determine the Palmyra signal correlation values as a function of period, correcting for the noise (which is a problem at low S/N), compare the correlation results to the MF results, develop an "F detector" detection theory with which to compare the detection capability of different array apertures, and determine the optimum array aperture with respect to both detection and azimuth estimation (using the azimuth estimation theory discussed in Blandford (1997)). This theory, by Shumway *et al.* (1999), is also given in this report in Appendix 1, and is extended there to include results for simple beamforming as well as for the case of optimum beamforming, which was given in Blandford (1997). We then show that the same aperture results are obtained if simple beamforming is used for azimuth estimation in place of optimum (weighted) beamforming, and also present some additional coherence data which also is consistent with MF. The paper closes with a summary and conclusions.

PALMYRA AND OTHER SMALL INFRASOUND ARRAYS, AND PALMYRA DATA

The 2.6 kt atmospheric event Tanana was detonated at 1.65°N, 157.28°W at 16:08:52 on 25 May 1962 as part of Operation Dominic. The shot point was south of Kiritimati Island, 1.87°N, 157.33°W (at shot time the island was a United Kingdom possession and was named Christmas Island).

Approximately 700 km to the northwest, on Palmyra Island, a US possession at 5.88°N, 162.08°W, the US Government in 1962 installed the temporary infrasound station "Small Fry." As seen in Figure 2, Palmyra is made up of a number of islands with a typical dimension of 1 km, connected by several man-made structures, erected just before WWII, within a reef approximately 3 km by 10 km.

Thus, although the original coordinates of the 1962, 3-element Small Fry array have not yet been recovered from archives, it seems plausible that the elements could be spaced at distances on the order of 1 km. As we shall see, this is supported by the observation that the maximum signal delay across the array is approximately 3 seconds. The existence of this small array is critical because data from it comprises almost all the atmospheric nuclear explosion data that is available at the lower limit of instrument spacings which are representative of the proposed infrasound arrays to be built for International Monitoring Community monitoring.

Perhaps unfortunately for our present purposes, the Small Fry array may have had linear pipe filters approximately 300 meters in length; it is believed that such filters were designed and became standard in US Government arrays soon after 1955 since the principal objective of the network was to detect 100 kt or greater explosions at distances >3000 kilometers. This length of pipe array would be about equal to the wavelength of a 1 Hz signal. The signal at 1 Hz would, therefore, likely be strongly attenuated along some azimuths, thus leading to an underestimate of S/N at $f \geq 1$ Hz and, therefore, to an underestimation of the capability of 1 Hz detection and azimuth estimation for arrays of instruments with pipe arrays of, say, 100 meters characteristic dimension.

An initial infrasound array was installed on Palmyra in 1951 for Operation Greenhouse. A February 1952 Final Report of the "Ascension Group" is the source of Figure 2. Reference to a navigation chart for Palmyra suggests that the four elements of the 1952 array were located at sites which can be described as:

(1) Strawn Island
(2) Aviation Island, 0.25 km East of the North end of the North-South Causeway
(3) NE end of Eastern Island
(4) Eastern end of Kaula Island, 0.2 km West of the South end of the North-South Causeway.

For this earlier array, the greatest separation was between elements 1 and 4, and was 4.5 km; and the least was between elements 2 and 3, and was 2 km. Thus, it is apparent that the 1962 Small Fry array must have been deployed differently from the 1951 array. There were also other small-to-intermediate size arrays deployed in 1951 at the Majuro Atoll, and at Eniwetok itself near

which the four explosions of operation Greenhouse were detonated. The 1952 data are currently being recovered and digitized.

Figure 3 shows the unfiltered waveforms of Tanana at Palmyra with "A-B" and "C-D" indicating two 100-second time windows in the signals which are used for analysis, and Figure 4 shows channel 3 filtered through a set of passbands centered at the periods indicated.

The Tanana signal in Figure 3 is somewhat misleading; it might seem that the time axis has been reversed, that the earliest times are on the right of the plot and that the signal first arrives in the C-D time interval. However, it is actually the case that the initial arrival is in the A-B window. The low noise level to the right is a coincidence; and this is seen in a later section by examination of the similar signal from the event Petit, which took place near Tanana and was also recorded at Palmyra on Small Fry. We will see that, although the signal is very similar, as would be expected, the amplitudes after the window corresponding to C-D are not low.

DATA ANALYSIS TECHNIQUES

To compute the cross correlations of the signals in Figure 3, we first align them in time, using the delays which give a maximum in the unfiltered trace cross-correlation for the C-D window shown in Figure 3. This window is chosen because it appears to have the highest S/N. To determine the alignment delays we note that the signal arrives first on channel 2. For maximum correlation, channel 1 must be moved 3.6 seconds to the left, and channel 3, 3.3 seconds to the left. In subsequent calculations of correlation, we calculate the correlation at these fixed offsets for both the A-B and C-D windows, and for all periods.

The noise mean-square covariances, needed to correct the correlation estimates as discussed below, were calculated for each channel over the window comprising the first 3 minutes of data in Figure 3. Cross-correlations were also calculated over these windows and were found to be randomly positive and negative, and not significantly different from zero, showing that there was no significant signal in the first 3 minutes so that the mean-square covariance estimates were unbiased.

The correlations are calculated using the above fixed delays for all periods, rather than adjusting the delay for maximum correlation at each period, because analysis suggests that, on the one hand, the hypothesis of a fixed delay cannot be rejected and that, on the other hand, at some periods the S/N is poor enough that using the maximum correlation as the signal correlation estimate would result in an positively biased estimate for correlation.

On the other hand, in the presence of noise, the normalized signal cross-correlation at a fixed delay will be biased low. This is because the single-channel covariances which are multiplied together (and the square root taken) in the denominator of the conventional cross-correlation estimator are biased above the value which they would have for signal alone in the absence of noise. On the other hand, the cross-variance term in the numerator is unbiased by the noise. This is because infrasound noise is uncorrelated with both the signal and with noise on other channels.

Assuming for convenience, without loss of generality (for unequal noise values we take A_s to be the square root of the product of the power of the two channels), that the noise has the same spectrum on all channels, then the correlation, ρ, is:

$$\rho = \frac{C_{ij}}{A_s} \qquad (2)$$

where C_{ij} is the cross correlation between two channels and where A_s is the autocorrelation. The signal cross-correlation corrected for noise, under the assumption that the noise is stationary and uncorrelated with the signal, is given by:

$$\rho_c = \frac{C_{ij}}{A_s - A_n} \qquad (3)$$

where A_n is the autocorrelation before the signal. Note that since statistical fluctuations are expected between the noise before the signal and the noise during the signal, it is possible for the noise-corrected signal correlation estimate to be greater than 1.0. Also, it is possible that the correlation estimate may be undefined. For low S/N, it may sometimes happen that the pre-signal mean-square noise estimate is greater than the estimate for mean-square signal plus noise. Thus, the estimate for the mean-square noise in the signal window may be negative.

To estimate detection thresholds, and standard errors of azimuth estimates at those thresholds, it is necessary to be able to predict the S/N and correlation for yields lower by a factor, A_f, than those events that provided the basic data.

We need estimates of the total signal power, the correlated signal power, and the uncorrelated signal power.

It is interesting to note that the uncorrelated signal power does increase the S/N of the beam in the time domain. If P is the number of channels in the beam, the uncorrelated power is reduced in the beam by a factor of 1/P in comparison to the correlated power. So this additional uncorrelated power is added to the correlated power after the arrival of the signal, enhancing the S/N over that due to the correlated power alone.

We see that the correlated signal power on a single channel of a channel pair is:

$$A_{s,c} = \rho_c \cdot (A_s - A_n) \tag{4}$$

and the uncorrelated signal power on a single channel of a channel pair is:

$$A_{s,uc} = (1 - \rho_c) \cdot (A_s - A_n) \tag{5}$$

To examine a case of a reduced amplitude source, we may multiply A_{sc} and $A_{s,uc}$ by the same suitable source strength factor, A_f, to obtain $A'_{s,c}$ and $A'_{s,uc}$; here uc and c refer to uncorrelated and correlated, respectively. Then, the correlation would be given by the cross-spectral power divided by the total power on either (equal power) single channel, comprising the sum of the correlated and uncorrelated signal power plus the noise power. Thus,

$$\rho' = \frac{A'_{s,c}}{A'_{s,c} + A'_{s,uc} + A_n} \tag{6}$$

would be the correlation between the same two channels for the same two signal waveform shapes, but with each amplitude changed by the factor, A_f, and embedded in the original noise, A_n.

For application to determine probability of detection and errors of azimuth estimates, using theoretical correlation estimates for reduced amplitude signals in the original noise, we also need the signal-to-noise on an individual channel, $(S/N)\text{-}_P$ Thus,

$$(S/N)'_P = (A'_{s,c} + A'_{s,uc})/A_n \qquad (7)$$

Table 1 gives the raw signal correlation and the correlation corrected for noise for the two windows seen in Figure 3 and for the bandpass limits illustrated in Figure 4. The actual calculations were performed using SAC2000 and following the formulas given in the previous section.

B (Hz) T (sec)	Cross-Correlation of Aligned Traces 1:2, 1:3, 2:3 Tanana at Palmyra (Small Fry)							
	Observed Signal Correlation				Corrected for Background Noise			
	Window A-B		Window C-D		Window A-B		Window C-D	
.025-0.1	-.02		.85		U		1.18	
20	.35	.29	.94	.85	4.3	U	1.36	1.30
0.05-0.2	.50		.72		1.3		1.2	
10	.34	.46	.88	.87	.54	.96	1.3	1.3
0.1-0.5	.72		.69		.90		1.04	
4	.62	.84	.59	.68	.80	.85	.81	.86
0.2-0.5	.64		.96		.81		1.4	
3	.70	.82	.63	.68	.83	.90	.98	.82
0.3-1.0	.58		.84		.67		.96	
2	.48	.69	.22	.60	.55	.72	.26	.64
0.5-2.0	.38		.71		.44		.77	
1	.28	.40	.02	.21	.35	.44	.03	.22

Table 1. Correlation Analysis of Signals in Figure 3

Since the signals arrive at channels 1 and 3 within 0.3 seconds of each other, we may assume that the vector between them was aligned nearly parallel to the wavefront and that they are, therefore, expected to have the lowest correlation, as shown by MF. The greatest delay, of 3.6 seconds, is between channels 1 and 2 and so we expect that these are oriented most perpendicular to the wavefront and would, therefore, have the highest correlation.

Examination of Table 1 shows that these expectations are born out. Assuming that all undefined correlation values, and corrected values greater than 1.0 (which are long-period) may be approxi-

mated by 1.0, and combining values for both windows, we have, for interpolation purposes, fit the correlation data with the expression 1-exp(-aT) where T is the period in seconds. We find, parallel to the wavefront a=0.39 sec^{-1}, and perpendicular to the wavefront, a=0.87 sec^{-1}, in accordance with the observation that for a fixed period and distance between elements the correlation is higher perpendicular to the wavefront than parallel to the wavefront. (We assume that even though the signals arrive at almost the same time at elements 1 and 3, the array is roughly in the shape of an equilateral triangle and that the spacing is approximately 1 km.)

Using these formulas, we may compare in Table 2 the interpolated results with the results predicted by MF. The predicted and observed values seem to be in reasonable agreement so we are encouraged to continue to use the formulas of MF in order to estimate signal correlation as a function of array element separation azimuth and distance, and as a function of signal period.

Comparison of Predicted and Observed Infrasound Correlation for Sensor Spacing of 1 km				
	Coherence Prediction, Mack and Flinn (1971) Δc=0.015 km/sec $\Delta \theta$=5°		Fitted Correlation Observations Tanana at Palmyra	
Signal Period (sec)	2	1	2	1
ρ parallel to wavefront	.87	.53	.54	.32
ρ perpendicular to wavefront	.96	.84	.82	.58

Table 2. Twelve (12) observations from T= 1 to 20 seconds, from Table 1, constrained to be <=1, were fitted to the expression 1-exp(-aT). a was found to be 0.39 parallel to the wavefront, and 0.87 perpendicular. Considering the scatter in the small amount of data which are available for analysis, the observations seem not inconsistent with the coherence predictions of MF although there is an indication that the observed correlation is less than predicted, which would suggest the use of smaller arrays than those suggested using the data of MF.

DETECTION THEORY

The theory required to estimate the errors in azimuth as a function of array aperture and S/N was given in Blandford (1997), Shumway *et al.* (1999) and is reproduced in Appendix I. However, evaluation of an array design or aperture should be evaluated in terms of detection as well as azimuth estimation. To evaluate detection from a quantitative point of view, we need a detection theory.

Because of the frequent, large, uncorrelated bursts of wind noise which appear on elements of infrasound arrays, the standard STA/LTA detectors conventionally used for seismic detection, cannot be used for infrasound detection; their use would result in a very high false alarm rate. Instead, detectors have been used for decades which rely on detecting the presence of the same signal on different channels of the array; that is, detectors which rely on the detection of correlation between the channels. See, for example, Jacobson (1957), Smart and Flinn (1971), McKissic (1996).

The "F detector" discussed by Smart and Flinn (1971) and by Blandford (1974) does, in fact, rely on correlation between sensors, and also has a detection theory which is firmly based in classical statistics.

The F detector detects on the ratio of the array beam power to the mean-over-channels residual power. The residual power is computed by squaring the result obtained by subtracting the beam from the aligned signal channel and then averaging over channels. The ratio, a ratio of chi-square statistics, is an F statistic.

When a signal arrives, the ratio of chi-squares increases for two reasons. First, the numerator increases because the beam signal power is added to the ongoing beam noise power. Second, if the signal is correlated, then when the beam is subtracted from each individual channel, the residual noise is the same as before the signal arrived, and the numerator remains the same so that the ratio increases.

However, if an uncorrelated signal or burst of noise arrives, then the beam will increase in amplitude, but by less than if the signal were coherent, and, in the numerator, subtracting the beam increases the residual. As a result, the numerator and denominator increase in parallel and the ratio remains much the same.

In the presence of signal, the ratio is distributed as non-central F. The cumulative integral of F from 0 to q with N_1 and N_2 degrees of freedom and non-centrality parameter λ is expressed as:

$$pF(q, N_1, N_2, \lambda) \tag{8}$$

where $N_1 = 2BT$ is the degrees of freedom for the numerator, where B is the bandwidth (for example one of those indicated in Table 1), and T is the length of the detection window over which the power is averaged. In this report, we take T=100 seconds, which Figure 3 shows to be suitable. For the denominator, $N_2 = (P-1)2BT$ where P is the number of elements in the array.

The non-centrality parameter, λ is given by $\lambda=2BT(S/N)_{beam}$, where $(S/N)_{beam}$ contains the correlated power (the true signal, S) and is the S/N on the beam.

For detection analysis, it is necessary to fix the false alarm rate. This corresponds to the probability of the F statistic fluctuating, in the absence of signal ($\lambda=0$), and exceeding a fixed threshold, q_T, in a period of time. We choose the rate to be one false alarm per day. This false alarm rate per beam would result in approximately 10 false alarms per day for a 200-meter aperture infrasound array which typically has 10 noise-independent beams. This number of false alarms is expected to result in very few false two-station network events per day. For the selected detection window of T=100 seconds (again, seen to be suitable in Figure 3), this corresponds to $1-pF(q_T, N_1, N_2, 0)=0.00116$. Solving for q_T for the varying values of B and for P=4 gives the values for q_T found in Table 3.

Detection and Location Parameters for CD Infrasound (1,2,3) km Aperture Arrays Derived from Mack and Flinn (1971) Correlations, and Power $(S/N)_p$ from Tanana as Observed at Palmyra, Reduced by a Factor of $A_f=1/25$.											
Tanana at Palmyra Signal Parameters						Theoretical Mean Signal Correlation,ρ, for Int'l Monitoring Community Arrays (all numbers)			Non-centrality Parameter $\lambda=2BT*(S/N)_{beam}$ for Int'l Monitoring Community Arrays, $A_f=1/25$ (all numbers)		
T_c (s)	B (Hz)	q_T	$\bar{\rho}$	ρ_c	S/N_P	1km	2km	3km	1km	2km	3km
20	.075	3.12	0.54	1.0	1.2	.998	.995	.99	1.62	1.62	1.62
10	.15	2.33	0.62	1.0	1.6	.995	.98	.96	14.9	14.6	14.3
4	.4	1.70	0.69	.87	3.8	.97	.89	.77	55.2	48.8	42.0
3	.3	1.84	0.74	.89	4.9	.95	.81	.63	41.6	34.8	26.5
2	.7	1.50	0.57	.63	8.1	.89	.63	.39	130	87.2	50.4
1	1.5	1.32	0.33	.38	13.2	.63	.22	.065	262	77.5	21.6

Table 3. Detection and Location Parameters for CD Infrasound

T_c is the center period for the detection filter passband with bandwidth B and time duration T=100 sec. q_T is the F detection threshold for one false alarm per day. $\bar{\rho}$ is the average observed correlation, which is estimated as the average over the data in columns 2-3 of Table 1 for the observed correlation between two traces.

(S/N)$_P$ is the power signal-to-noise ratio on a single channel; it may be derived starting with the relation, for the observed correlation between two traces

$$\bar{\rho} = \frac{correlated\,signal}{uncorrelated\,signal + noise + correlated\,signal} \qquad (9)$$

where we may take the correlated signal as equal to the signal power S times the correlation corrected for background noise, ρ_c. (We may estimate ρ_c as the average over columns 4-5 in Table 1, with 1.0 replacing all values greater than 1.) Then, the uncorrelated signal may be determined as $(1-\rho_c)$ times S.

Using these relations, one may obtain the formula,

$$\left(\frac{S}{N}\right)_P = \frac{\bar{\rho}}{\rho_c - \bar{\rho}} \qquad (10)$$

This formula is used in Table 3 to produce column 6 from columns 4 and 5. The approximation here is that we average over relative propagation azimuths and assume that all three sensor spacings are the same for the observing array at Palmyra.

$(S/N)_P$ in Table 3 is one of the critical pieces of information determined by this analysis of Tanana as recorded at Palmyra. It gives an estimate of the single-sensor power S/N as a function of frequency for a source, distance, and system of interest.

It should be noted that, as mentioned previously, due to the loss of signal amplitude created by 300-meter pipe arrays, it could be that this value of S/N at 1 Hz is underestimated compared to that which would be possible for a more ideal system. In addition, it is possible that the space-filling, 100m aperture pipe arrays currently being considered for the International Monitoring Community arrays may improve S/N over that found here.

However, going ahead and using these results, together with the theoretical relations for correlation as a function of period and element spacing from MF (also verified by the Tanana-Palmyra data), we will calculate S/N on the beam, detection probability, and azimuth estimation precision for arrays of different designs looking at the Tanana signal scaled to simulate a smaller yield.

The columns headed "Theoretical Mean Signal Correlation" in Table 3 are determined using the parameters Δc =0.015 km/sec and $\Delta\theta$ =5° and the relation of MF to determine the mean correlation for signals at infinite S/N at International Monitoring Community arrays with apertures of 1, 2, and 3 km.

Note that the theoretical values for a 1 km array in Table 3, column 7, are larger than are the corrected observed values in column 5, ρ_c. This is appropriate because three of the six intersensor

distances in a 4-element International Monitoring Community array (an equilateral triangle, 1 km on a side, plus a central element) of this size are 0.43 km; whereas the 3-element Small Fry array had only three spacings, each likely was approximately 1 km. Also, we have noted above, in discussion of Table 2, that the observed correlations appear to be somewhat lower than predicted.

For detection analysis purposes, it is necessary to calculate the non-centrality parameter, λ. The new element in this calculation is given by the (S/N) on the beam. To be consistent with the classical development of the F detector, Shumway (1983), which assumes that the signal is perfectly correlated, we assume that only the correlated signal power will count as S. Thus, counting the uncorrelated S as noise, $(S/N)_{beam}$ is given for a 4-element array by

$$(S/N)_{beam} = \frac{\rho \cdot A_f \cdot (S/N)_P}{\frac{1}{4} \cdot [(1-\rho) \cdot A_f \cdot (S/N)_P + 1]} \tag{11}$$

where A_f is the factor giving the reduction of signal power; for Table 3, $A_f = 1/25$, ρ is the average corrected signal correlation for the array (columns 7-9 in Table 3). This is equivalent to (1/25)th of the yield or 0.104 kt. We test capability for this low yield in order to evaluate in a yield region where there are significant operational differences between different arrays sizes. For substantially larger yields, all arrays would perform adequately at this distance, and for much smaller yields, no arrays would perform adequately.

DETECTION AND AZIMUTH ESTIMATION RESULTS

Using the parameters determined in Table 3, together with the detection theory outlined in the previous section, and with the azimuth estimation theory in Blandford (1997) (see also Appendix I), we obtain the results in Table 4.

	Detection and Location Estimates for CD Infrasound (1,2,3) km Aperture Arrays Using Parameters Derived from Mack and Flinn (1971), and the Event Tanana as Observed at Palmyra. Estimates for the Event Tanana as Observed at Palmyra with Amplitude Reduced by a Factor of 5.								
T_c(sec)	Beam Visual Amplitude (S/N) (rms/rms)			Probability of Detection With F using Simple Beam PD			Azimuth Estimate with Optimum Weighted Beam Standard Error, σ_θ °		
	1 km	2 km	3 km	1 km	2 km	3 km	1km	2 km	3 km
20	1.09	1.09	1.09	.006	.006	.006	20.1	10.1	6.8
10	1.12	1.12	1.12	.012	.012	.012	6.10	3.16	2.23
4	1.26	1.26	1.24	.34	.31	.25	1.04	.69	.62
3	1.33	1.31	1.29	.39	.32	.22	.89	.68	.63
2	1.49	1.44	1.37	.998	.977	.78	.42	.36	.36
1	1.66	1.46	1.36	1.0	.98	.41	.21	.31	.66

Table 4. Detection and Location Estimates for CD Infrasound

In Table 4, T_c is the center period for the detection filter passband. Detection and azimuth estimates are for a time window of 100 seconds. The "Visual" amplitude in columns 2-4 is computed by dividing the estimate for the beam noise power in front of the signal into the sum of the beam noise plus correlated signal power plus 1/4 the uncorrelated signal power (for a 4-element array), and then taking the square root.

The probability of detection is computed using the Splus statistical package pF subroutine which is suitable for a correlation F detector. A false alarm rate of one per day is specified along with a signal with 1/25th the power (yield~0.104kt) of Tanana at Palmyra. The azimuth estimate was calculated from the formulas in Appendix I using a Matlab analysis package routine, fsnewth.m, written by the author.

Calculation of azimuth error, of course, presupposes detection and also presupposes that subsequent analysis has selected the proper time window over which to estimate the azimuth. Thus, if

detection probability is low, the significance of the azimuth estimate is questionable. Examination of Table 3 appears to suggest that one should construct 1 km aperture arrays and detect at 1 Hz. Note that the best detection and azimuth estimate for this signal is found at 1-second period for a 1 km aperture array.

For 1 and 2 km aperture arrays, the best detection is found at 1-second period. For 3 km aperture arrays, the best detection is found at 2-second period.

Using the best period for detection for each aperture array, we may find the yield which gives 90% probability of detection for a fixed false alarm rate of one per day. The result is 0.032, 0.078, and 0.124 kt for 1, 2, and 3 km aperture arrays, respectively. Thus, a 1 km aperture array will detect 1/2.4 the yield as a 2 km aperture array, and 1/3.9 the yield as a 3 km aperture array.

The theory and expressions for the azimuthal error when simple beamforming is used instead of optimal beamforming are also given on the last page of the Appendix. Perhaps surprisingly, both the theory and the expressions are somewhat more complex for simple beamforming. However, again the expression for the azimuthal error has been computed for simple beamforming using the Matlab subroutine, bfsnewth.m (see Appendix), also written by the author.

In the last row of Table 4, for 1-second period, the azimuthal error in degrees for (1, 2, 3) km aperture for simple beamforming would be (0.33, 1.00, 1.32) instead of the (0.215, 0.31, 0.66) seen in the table, which is for optimum processing. For 2-second period, the values are (0.44, 0.51, 0.88) as compared to (0.42, 0.36, 0.36), and for longer periods, the differences are 30% or less.

Thus, for the optimum 1 km aperture array, there is only a 1.5 factor (0.33/0.215) advantage in azimuth precision to using the optimum azimuth estimation process in preference to fk beam-forming at the optimum detection period (1 sec), while, for 2 km and 3 km aperture arrays, the advantages are factors of 3.2 (at 1 sec) and 2.4 (at 2 sec), respectively.

Thus, the 1 km aperture array offers an advantage in processing in that there is a lesser require-ment for processing that is more sophisticated than simple beamforming to obtain the full benefit of the data than there is for the 2 km and 3 km arrays.

Note also that we have used as a detector the F statistic on a simple beam. It may be that the detection performance of the larger arrays could be improved by an optimum detector which took account of the loss of signal coherence. In a qualitative sense, such a detector would, presumably, detect to some degree on the sum of the power at each sensor. Such a detector would, however, likely be very vulnerable to the bursts of incoherent noise which are characteristic of infrasound data. Thus, again, we are brought back to using the smaller 1 km aperture array.

Of course, we must emphasize that all these conclusions rest on the correlation predicted by Mack and Flinn (1971), which was confirmed by Tanana, and on the observed (S/N) at a single sensor as a function of frequency for the event Tanana as seen at Palmyra. Further data is sorely needed.

ADDITIONAL CORRELATION DATA

The data for the event Tanana as recorded at Small Fry is the best data which I have been able to acquire for the purpose of testing whether or not the MF data could be extended to shorter periods and shorter distances between sensors.

However, there are some further data which are consistent with the Tanana-Small Fry data. In Figure 5, we see the event Petit, also recorded at Tanana. Analysis of the same signal windows as seen in Figure 3 gave similar results but with larger variation.

Figure 6 shows Petit as recorded at a 10-km aperture array at Oahu, a distance of approximately 2200 km. Unfortunately, the archived signal did not include a portion of uncorrelated noise before the signal arrival so that it was not possible to determine the true correlation values for these signals, only a lower value. These values, together with the theoretical MF values, are seen in Table 5 below.

Comparison of Observed and Theoretical Infrasound Signal Correlations							
Period (sec)		20	10	4	3	2	1
10 km spacing, Petit, 2.2 kt, at Oahu (~2200 km)							
Perpendicular to wavefront, elements 1-2	Observed (raw) (:13:50-:15:30 window)	>.91	>.56	>.29	>.35	>.13	>-.09
	Theoretical	.96	.84	.24	.05	~0	~0
Parallel to wavefront, elements 1-3	Observed (raw) (:13:50-:15:30 window)	>.68	>.41	>-.15	>-.28	>-.25	>-.09
	Theoretical	.87	.53	.22	.03	~0	~0

Table 5. Signal Correlation Comparison

If the negative values of correlation parallel to the wavefront for 4, 3, 2, and 1-second periods in Table 5 can be taken to indicate that the standard errors of the Oahu correlation estimates are ~0.25, then the theoretical (Mack and Flinn, 1971), and observed data seem not inconsistent, although there is a suggestion that, for estimates perpendicular to the wavefront, the observed correlations are greater than the theoretical.

Figure 7 shows the White Sands 19 November 1997 10-ton conventional explosion as seen at the TXAR infrasound array. In general, the S/N is fair. Figure 8 shows the 01 channel filtered through several passbands, and we see that a signal appears to be present between 20 and 1/2 second period.

The White Sands event is approximately 450 km to the northwest, such that only the 1.1 km interval between elements 01 and 02 is roughly perpendicular to the wavefront. The intervals (01 - 03), (01 - 09), and (03 - 09) are roughly parallel to the wavefront and are 0.8, 1.5, and 2.0 kilometers in length, respectively.

Table 6 gives correlations for these distances, calculated in the same way as for those in Table 1 and for a 200-second window surrounding 18:27 as seen in Figures 7 and 8.

Cross-Correlation, ρ_c, corrected for noise, of Aligned Traces White Sands, 10 tons, at TXAR 01:02 perpendicular to wavefront, others, parallel		
B (Hz) T (sec)	perpendicular interval=1.1 km 01:02	parallel interval=0.8 km 01:03
	parallel interval=1.5 km 01:09	parallel interval=2.0 km 03:09
2.0-4.0 .5	.75 .79	54 .46
1.0-4.0 0.7	.97 .89	.83 .88
0.5-2.0 1.5	.97 .97	.97 .98

Table 6. Correlation Analysis of Signals in Figures 7 and 8 for Four Different Sensor Pairs.

Periods given in Table 6 are the observed dominant period of the signal as measured after filtering. It is apparent that only correlations greater than 0.97 would be observed for periods greater than 1.5 seconds.

At periods shorter than 0.5 seconds, the S/N was poor, as can be seen in Figure 8. This is for a small (10 tons, 0.005 kt) shot, short distances, and with a hose array with a diameter of only 20 meters. Thus, it seems unlikely that higher frequencies will be useful, given the capability at lower frequencies, for detection or azimuth estimation of larger explosions at larger distances. It may possibly be that the higher frequencies would be useful for discrimination if they are generated in greater proportion by nonexplosive sources.

It is important to emphasize that these high correlation values would be lower if not corrected for noise. For example, the 0.98 value for the 1.5-second period for the 03:09 element pair separated by 2 km parallel to the wavefront would be 0.89 without correction; still quite high, of course.

Comparison of the squared values of the 1.5 second correlations with Figure 1 shows that such high correlations at distances between sensors of 1-2 km would only be obtained, with MF parameters, at periods of 10 seconds. This implies, roughly, that the azimuth and phase velocity variance determined by MF would have to be reduced by about a factor of 5 in order to be applicable to these regional signals.

One interpretation of this result might be that a one-hop signal, present at closer distances, does not have the azimuthal and velocity dispersion that a multi-hop signal has.

If true, this result emphasizes that results appropriate for 1000-2000 km detection and azimuth estimation are unlikely to be obtained by analysis of records from 500 km distances. Further work is required.

SUMMARY AND CONCLUSIONS

It seems likely that the optimum design for infrasound arrays for detection and location of 1 kt nuclear explosions at 1000-2000 km should be 1 km aperture arrays, and that detection processing should be concentrated in the neighborhood of 1 Hz. This conclusion is, if anything, likely to be strengthened by future analyses since the 1 Hz signal recorded at Small Fry was likely degraded in S/N by the large aperture pipe array.

There remains a paucity of data for a few kiloton explosions recorded at 1000-2000 km. There are some additional White Sands 4 kt conventional explosion data recorded at great distances, and substantial efforts to recover that data would be worthwhile. At AFTAC, Dean Clauter (personal communication) is striving to recover from the archives further nuclear explosion infrasound data recorded at small Pacific Island arrays. These data should be analyzed to ensure that the above conclusion is reliable.

It would appear that smaller explosions at closer distances will also have optimum detection at 1 Hz, and that the correlation will be excellent at 1 Hz for a 1 km aperture array, so that location accuracy should be excellent. It might be that a higher aperture array would give better location for these closer distances, but this is not likely to be a serious International Monitoring Community problem.
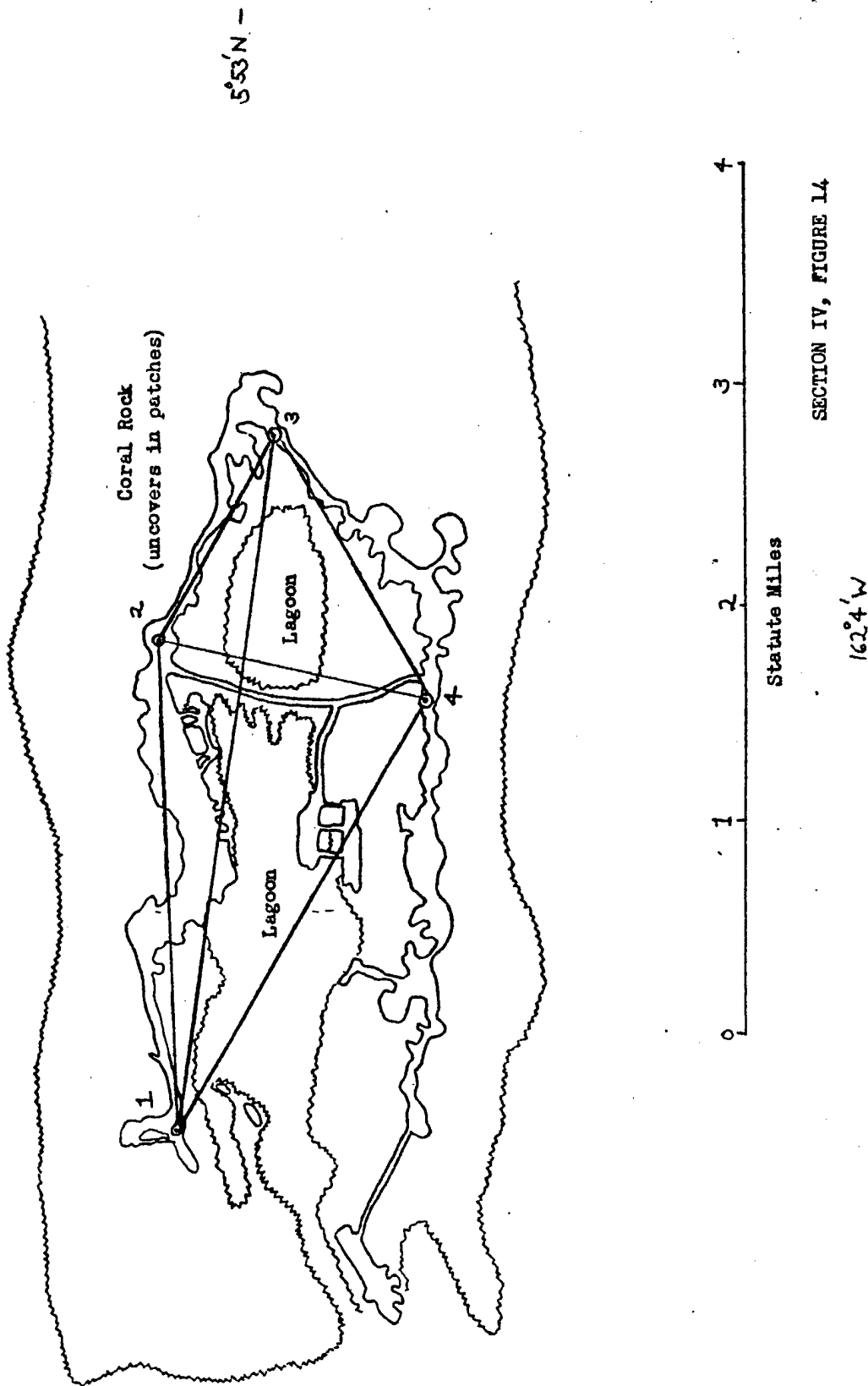
REFERENCES

Blandford, R.R. (1997). Design of Infrasonic Arrays, AFTAC-TR-97-013, Air Force Technical Applications Center, Patrick AFB, Florida.

Blandford, R.R. (1974). An automatic event detector at the Tonto Forest seismic observatory, *Geophysics*, **39**, 633-643.

Bonner, J., E. Herrin, and G.G. Sorrels (1997). Regional discrimination studies: Phase III, PL-TR-97-2064, Southern Methodist University/Phillips Laboratory.

Jacobson, M. (1957). Analysis of a multiple receiver correlation system, *J. Acoust. Soc. Am.*, **29**, 1342-1347.

Mack, H., and E.A. Flinn (1971). Analysis of the spatial coherence of short-period acoustic-gravity waves in the atmosphere, *Geophys. J. R. Astr. Soc.*, **26**, 255-269.

McKissic, M. (1996). Infrasound and the infrasonic monitoring of atmospheric nuclear explosions: An annotated bibliography, PL-TR-96-2282, DOE/Phillips Laboratory.

Shumway, R.H., S. Kim, and R.R. Blandford (1999). Nonlinear estimation for time series observed on arrays. In Asymptotics, Nonparametrics, and Time Series, S. Ghosh, Editor, Marcel Dekker.

Shumway, R.H. (1983). Replicated time series regression: An approach to signal estimation and detection. In Brillinger, Krishnaiah ed., *Handbook of Statistics, Vol. 3, Time Series in the Frequency Domain*, Amsterdam: North Holland.

Smart, E., and E.A. Flinn (1971). Fast frequency-wavenumber analysis and Fisher signal detection in real-time infrasonic array data processing, *Geophys. J. R. Astr. Soc.* **26** 279-284.

FIGURES
2 - 8

PALMYRA ISLAND

Coral Rock
(uncovers in patches)

3

2

Lagoon

Lagoon

4

1

5°53'N —

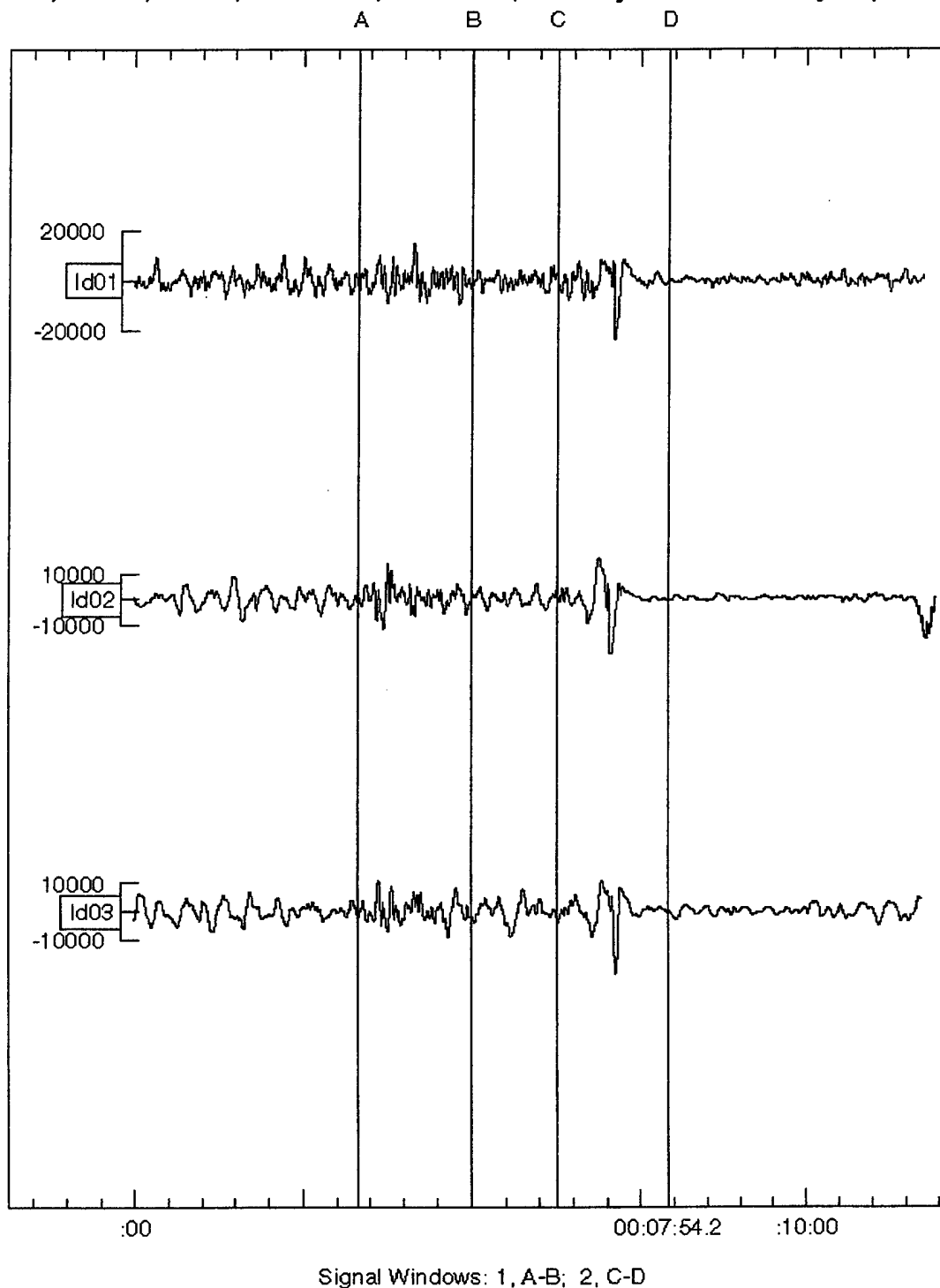0   1   2   3   4

Statute Miles

162°4'W

SECTION IV, FIGURE 14

Figure 2. Map of Palmyra Island, 5.88°N, 162.08°W which was the site of the Small Fry infrasound array which recorded the signals of the event Tanana on 25 May 1962. Tanana was detonated 25 km south of Kiritimati (Christmas) Island at 1.65°N, 157.28°W, a distance of 708 km to the SE of Palmyra. The array indicated on the map is not the 1962 3-element Small Fry array, whose coordinates are at present unknown, but is instead a larger array installed in 1951.
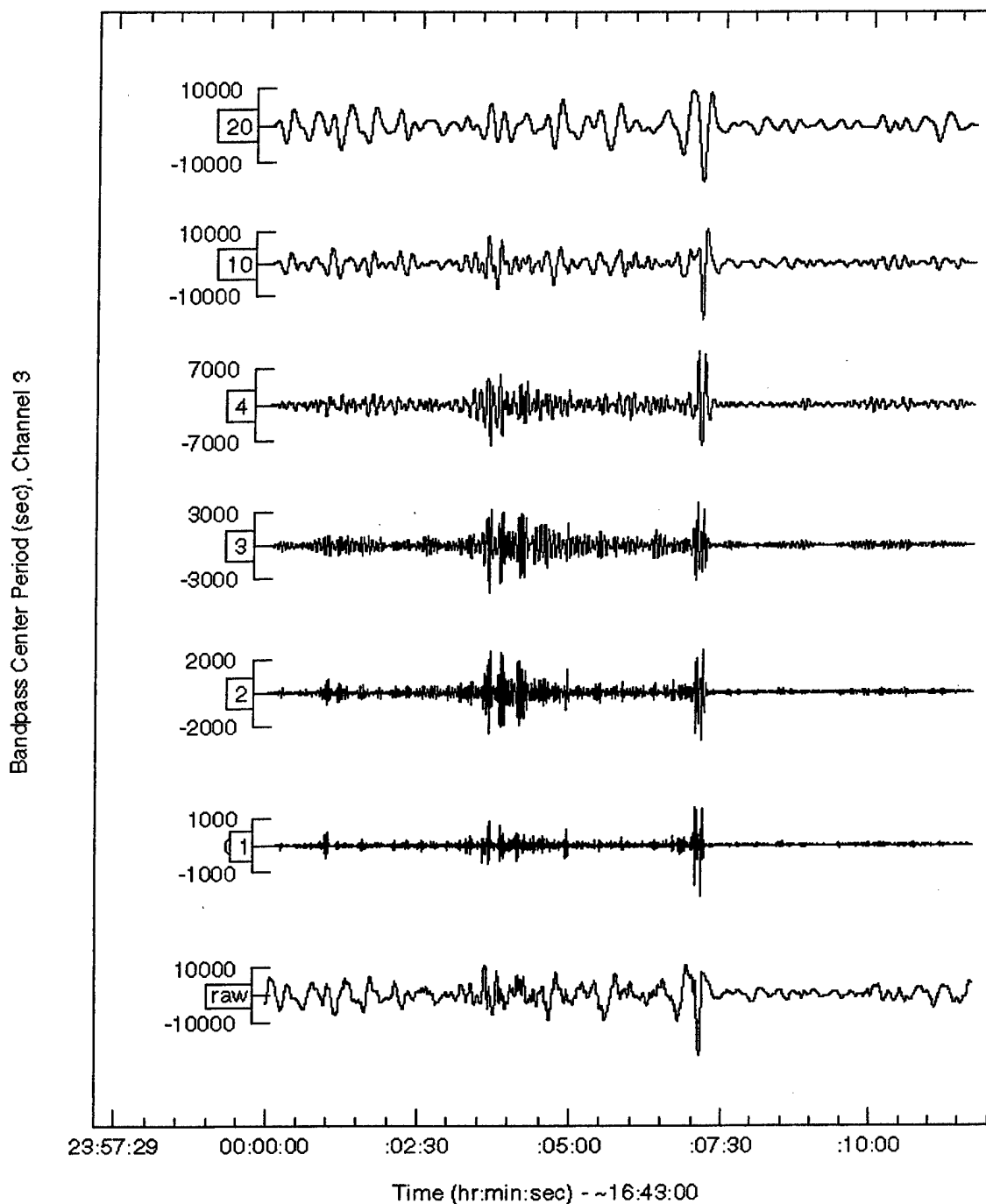
22

Figure 3. Unfiltered waveforms of Tanana as recorded at Palmyra. The first arrival is shortly after the vertical line "A". The two signal windows, of 100 seconds each, are the A-B and C-D intervals. A 180-second noise window before "A" was used to estimate noise.

Tanana, 2.6 kt,1.65N, 157.28W, 16:08:52, 25 May 1962 at Palmyra (Small Fry)

Figure 4. Channel 3 of Tanana as recorded at Palmyra, filtered through passbands with center periods as indicated. The S/N is roughly equal over the passbands; however, as discussed in the text, the shorter periods have the advantage of greater bandwidth for detection and azimuth estimation so long as signal correlation is adequate for the array sensor spacing.
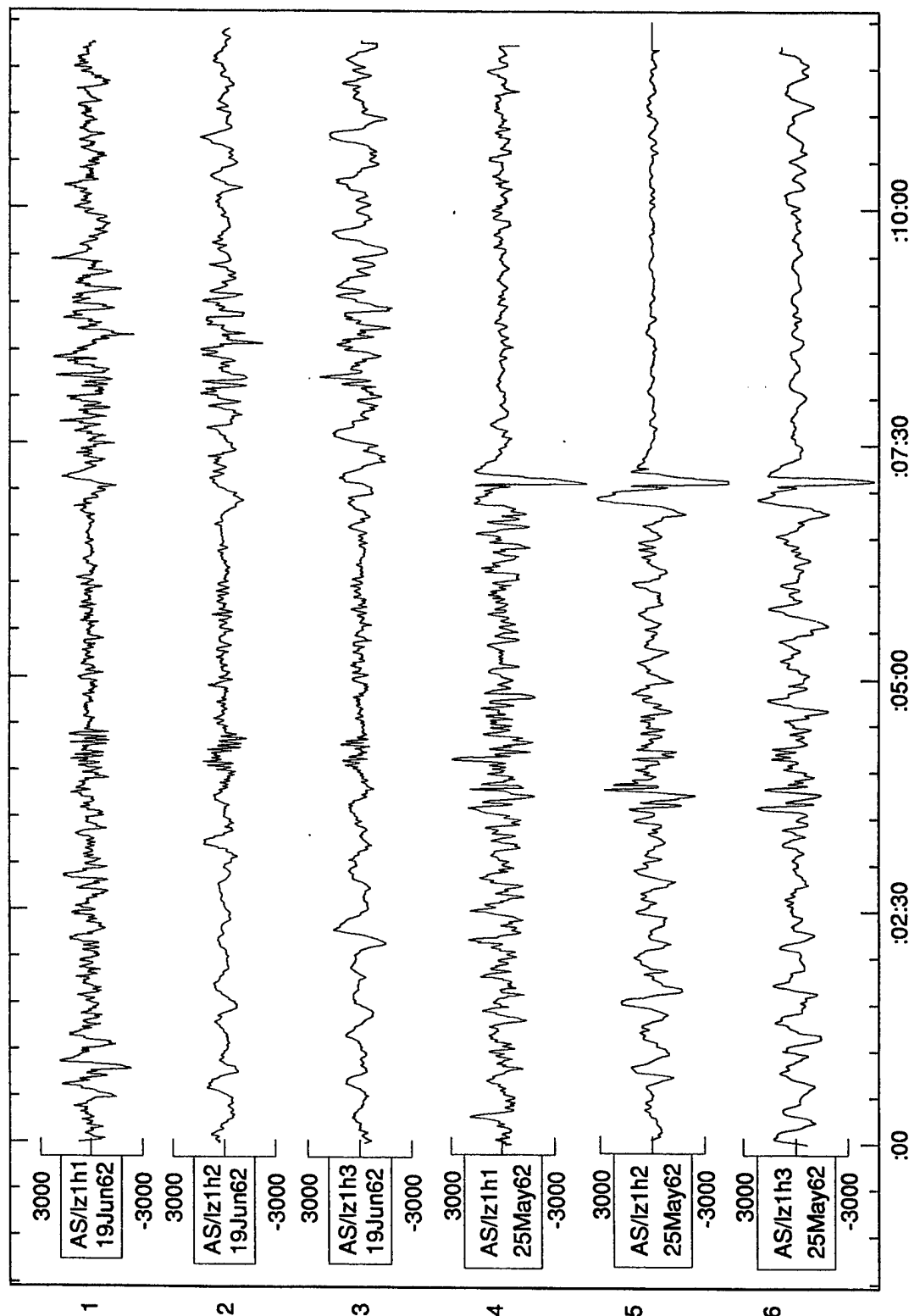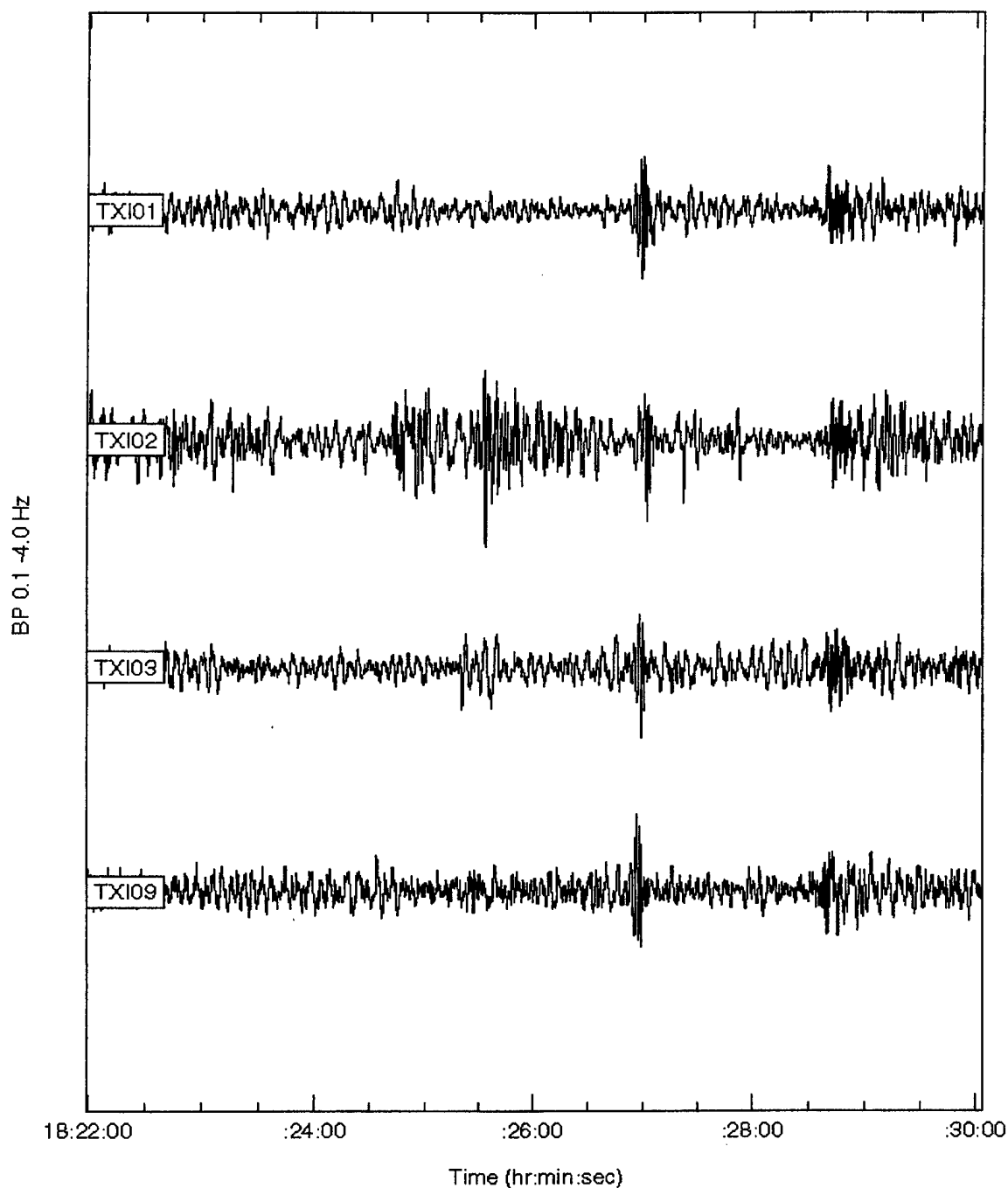
Figure 5. Petit, 2.2 kt, (code-name Pool) and Tanana, 2.6 kt, (Tan) as recorded at the array Small Fry on Palmyra. The figure shows that Tanana had a better S/N ratio and that the sharp reduction in noise amplitude after the second arrival for Tanana was a coincidence which did not occur for Petit. The poorer S/N for Petit made it possible only to show that Petit was not inconsistent with the results for Tanana; Petit could not substantially improve the correlation, and comparative S/N as a function of period, estimated with Tanana.

25

Petit, ~15:00, 19 June, 1962 at Oahu (Grape Sugar), ~2200 km
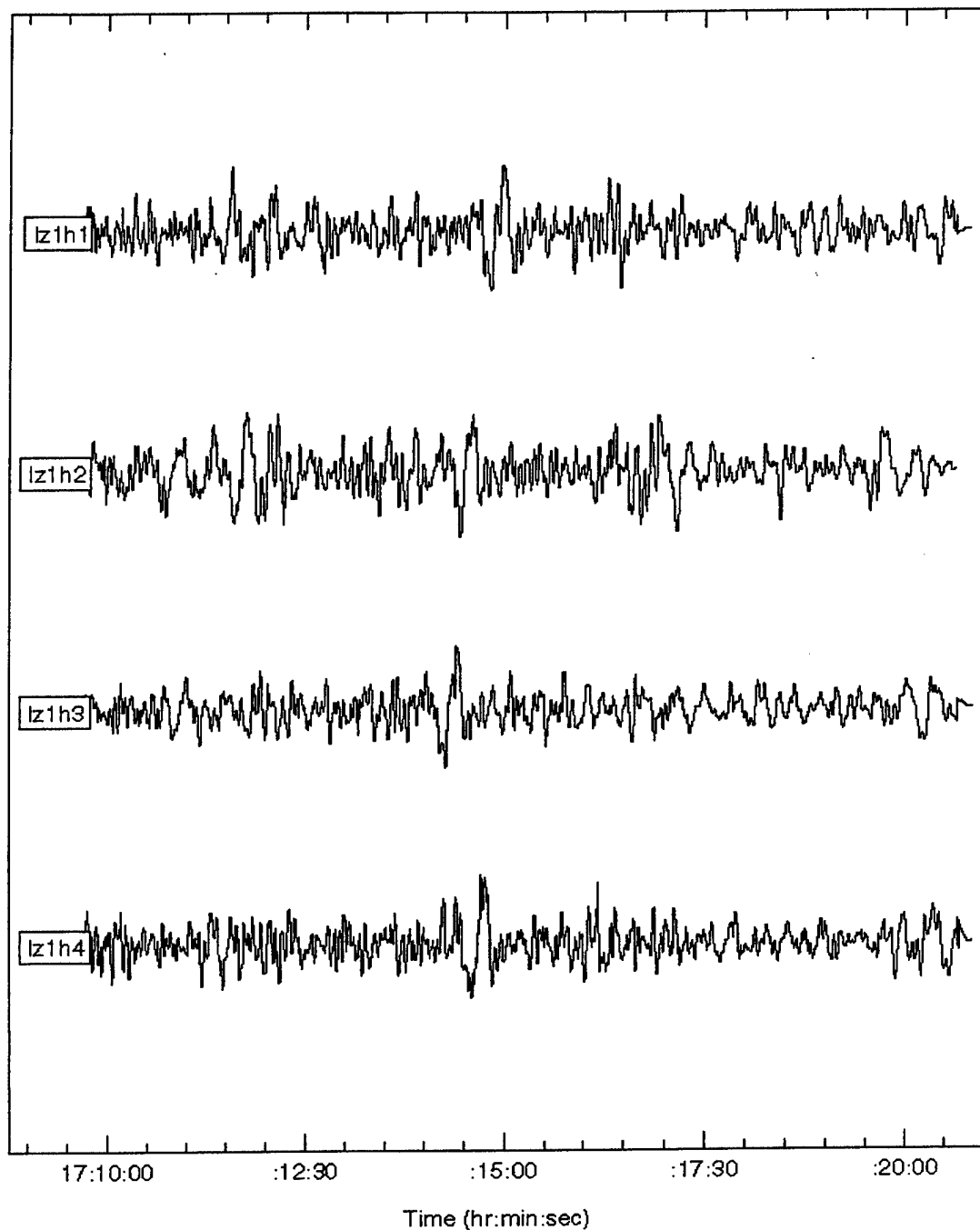
**Figure 6.** Petit, 2.2 kt, as recorded at the Grape Sugar array on Oahu, approximately 2200 km distant. Analysis shows substantial correlation at the beginning of the window, which was digitized from an archival reproduction, so that no noise window is available with which to calculate corrected correlations. The typical dimension of the array is 10 km and delays are correspondingly as great as 30 seconds.

26

Figure 7. The White Sands, New Mexico, simultaneous conventional explosion of 0.005 kt on 19 November 1997 as recorded at the TXAR infrasound array at a distance of approximately 450 km. Note that channel 1 has lower noise than the other channels, while channel 2 has higher noise. Unequal conditions of this sort prevail at many infrasound arrays, and detection and azimuth estimation techniques should be developed to allow for these differences.

27

White Sands Explosion, 19 Nov 1997,TXI01,
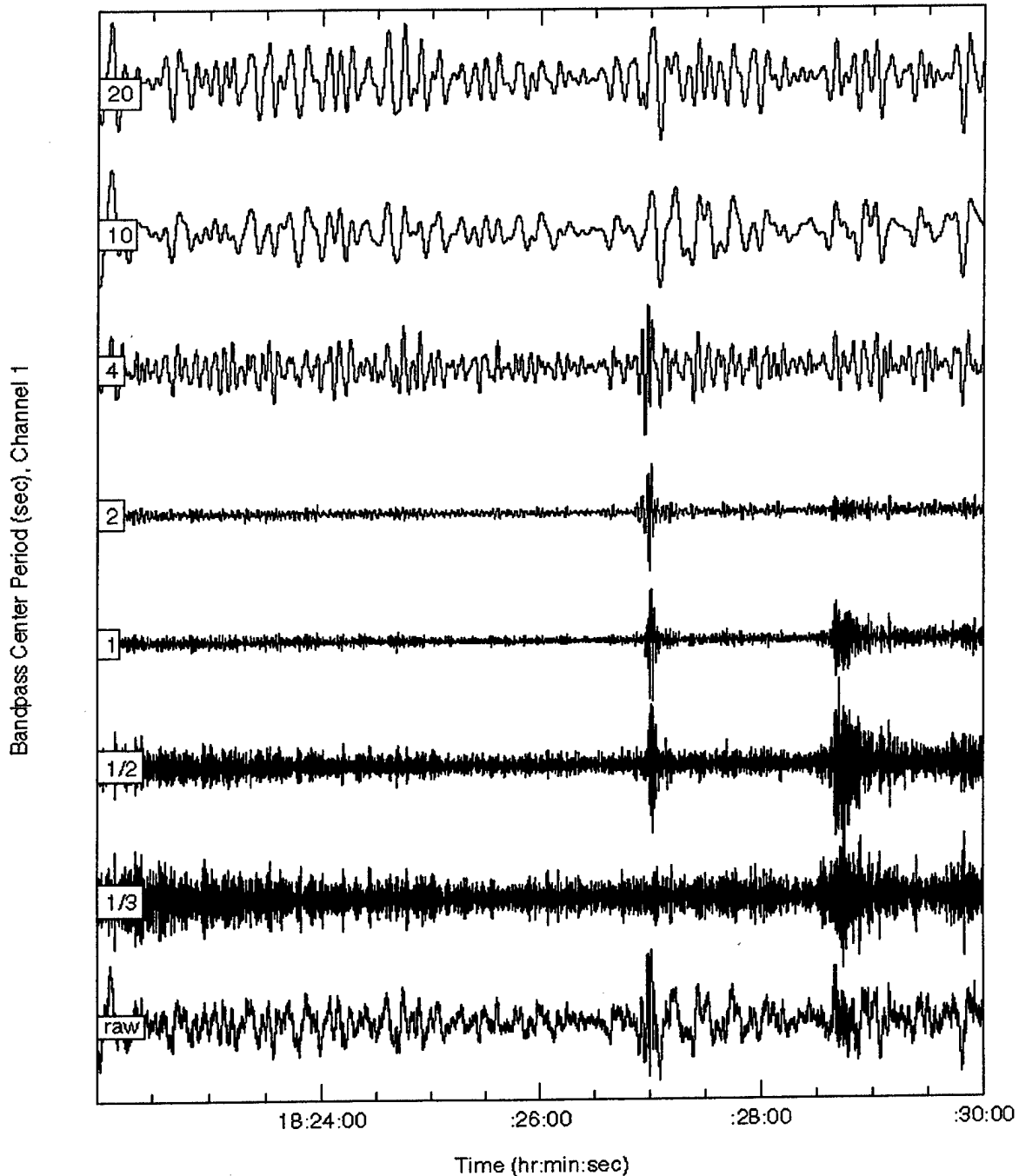
Figure 8. Channel 1 of TXAR from the White Sands event, the lowest noise channel shown in Figure 7, filtered through passbands with center periods as indicated. The highest S/N is for periods of 2 and 1 seconds and, as discussed in the text, the correlation is over 0.9 for both periods (much higher for this "regional" signal than would be predicted by the parameters estimated by Mack and Flinn (1971) for longer paths). Thus, we expect that the best detection and azimuth estimation would occur at 1 second since, at that period, greater bandwidth is available.

APPENDIX

APPENDIX: Detection and Estimation for Propagating Stochastic Signals

Robert H. Shumway

Division of Statistics

University of California, Davis

October 1, 1996

1. The Stochastic Signal Model

In general a model for a collection of signals, observed at an array of N sensors whose response is denoted by $y_j(t), j = 1, \ldots, N, t = 0, 1, \ldots, T - 1$ is

$$y_j(t) = s_j(t - T_j(\theta)) + v_j(t) \tag{1}$$

where $s_j(t)$ are random signals, assumed to be different on each channel, and $T_j(\theta)$ are time delays induced by a propagation pattern indexed by the wavenumber coordinates $\theta = (\theta_1, \theta_2)'$ which are nonlinearly related to the velocity and azimuth of a propagating plane wave. We assume that the signals are stationary processes and denote the $N \times N$ spectral matrix by $f_s(\nu), -.5 \leq \nu \leq .5$. The noise processes are often assumed to be independent and identically distributed across the array but have a stationary correlation structure over time; we denote the common spectral density by $P_n(\nu)$. with ν denoting frequency in cycles per unit time. The time delays are expressed in terms of the physical locations $r_j = (r_{j1}, r_{j2})'$ of the sensors as

$$T_j(\theta) = \frac{r_j' \theta}{\nu} \tag{2}$$

over a set of frequencies ν where the assumption (2) can be made. We may also consider a version of (1) which assumes a common stochastic signal, say $s(t)$, on all channels, i.e.

$$y_j(t) = s(t - T_j(\theta)) + v_j(t), \tag{3}$$

and we refer to this as the *perfect correlation model.*

It is conventional to consider the above model in the frequency at a collection of L frequencies, say $\nu_1, \ldots, \nu_L$ over which the signal and noise spectral matrices are constant, say at f_s and $P_n I_N$ where I_N denotes the $N \times N$ identity matrix. Taking discrete Fourier transforms yields the approximation

$$Y_{j\ell} = A_j(\theta) S_{j\ell} + V_{j\ell} \tag{4}$$

over a set of frequencies $\ell = 1, \ldots, L$, where

$$\begin{aligned}
A_j(\theta) &= \exp\{2\pi i \nu T_j\} \\
&= \exp\{2\pi i r_j' \theta\}.
\end{aligned} \tag{5}$$

This means that we may write a vector form of (4) in the frequency domain as

$$\mathbf{Y}_\ell = G(\theta)\mathbf{S}_\ell + \mathbf{V}_\ell, \tag{6}$$

where $\mathbf{Y}_\ell, \mathbf{S}_\ell$ and $\mathbf{V}_\ell$ are vector transforms of the observed data, signal and noise respectively and

$$G(\theta) = diag\{A_1(\theta), A_2(\theta), \dots, A_N(\theta)\} \tag{7}$$

is an $N \times N$ matrix with the $A_j(\theta)'s$ down the diagonal. The spectral matrix of the observed vector $\mathbf{Y}$ is clearly

$$f_y(\theta) = G(\theta)f_s G^*(\theta) + f_n I_N \tag{8}$$

where C^* denotes the complex conjugate transpose of the matrix C. The mean value of the vector $\mathbf{Y}_\ell$ is zero since the signal and noise processes are assumed to have zero means.

A special case of interest is the perfectly correlated signal where we assume that or equivalently, that the model (3) is

$$Y_{j\ell} = A_j(\theta)S_\ell + V_{j\ell}, \tag{9}$$

which is stacked in the form

$$\mathbf{Y}_\ell = \mathbf{g}(\theta)S_\ell + \mathbf{V}_\ell \tag{10}$$

where

$$\mathbf{g}(\theta) = (A_1(\theta), A_2(\theta), \dots, A_N(\theta))' \tag{11}$$

now becomes an $N \times 1$ vector and the spectral matrix becomes

$$f_y(\theta) = P_s \mathbf{g}(\theta)\mathbf{g}^*(\theta) + P_n I_N. \tag{12}$$

It should be noted that the model discussed in this note differs from the usual case where we regard the signal as being fixed and unknown, but identical between sensors. In that case, the model looks exactly like Equation (9), with the signal assumed to be fixed and unknown. Hence the vector $\mathbf{Y}$ in this case will have mean $\mathbf{g}(\theta)S$ and spectral matrix $P_n I_N$. The theory for various proposed estimators in this case has been covered in Hinich and Shaman (1972), Hinich (1981), Wu (1982), Shumway (1982) or Brillinger (1985).

For the stochastic signal case, we consider estimation of the signal and its mean square error in the next section and then move to sections on maximum likelihood detection and estimation in the following sections.

2. Signal Estimation

For the stochastic signal case, it is clear that, in the frequency domain, the signal estimation problem can be solved under either the linearity or Gaussian assumptions by computing the conditional expectation of the signal given the data under the Gaussian assumption. We consider the two cases corresponding to models assuming perfect correlation and more general correlation structures.

31

2.1 Signal Estimation: The Perfectly Correlated Signal

The perfectly correlated case has also been considered by Harris (1990). Suppose we consider the model given by (9) under the assumptions on the noise and spectral matrices summarized in (11). Using the Gaussian assumptions leads to estimating S_ℓ by

$$
\begin{aligned}
\hat{S}_\ell(\theta) &= E(S_\ell|\mathbf{Y}_\ell) \\
&= P_s \mathbf{g}^*(\theta)\Big(P_s \mathbf{g}^*(\theta)\mathbf{g}(\theta) + P_n I_N \Big)^{-1} \mathbf{Y}_\ell \\
&= \Big(\mathbf{g}^*(\theta)\mathbf{g}(\theta) + \frac{P_n}{P_s} \Big)^{-1} \mathbf{g}^*(\theta)\mathbf{Y}_\ell \\
&= \frac{\mathbf{g}^*(\theta)\mathbf{Y}_\ell}{N+r},
\end{aligned}
\tag{13}
$$

where $\mathbf{g}^*(\theta)\mathbf{g}(\theta) = N$ from (5) and (11) and

$$
r = \frac{P_n(\nu)}{P_s(\nu)}
\tag{14}
$$

is the inverse of the signal to noise ratio. The result exhibits the signal estimator as the beam $\mathbf{g}^*(\theta)\mathbf{Y}$ adjusted by a multiplier that depends on the number of elements N and the noise to signal ratio r. The mean square error of the signal estimator reduces to

$$
\begin{aligned}
\sigma^2(\theta) &= P_s - P_s \mathbf{g}^*(\theta)\Big(P_s \mathbf{g}(\theta)\mathbf{g}^*(\theta) + P_n I_N \Big)^{-1} \mathbf{g}(\theta)P_s \\
&= P_n \Big(\mathbf{g}^*(\theta)\mathbf{g}(\theta) + \frac{P_n}{P_s} \Big)^{-1} \\
&= \frac{P_n}{N+r}.
\end{aligned}
\tag{15}
$$

It is clear that the estimated signal is basically the beamformed estimator $\mathbf{g}^*(\theta)\mathbf{Y}_\ell$ and that the variance goes down by a factor that is weighted by the number of sensors plus the inverse of the signal to noise ratio.

2.2 Signal Estimation: The General Correlated Signal

For the general stochastic signal case, it is convenient to assume that the transforms are complex Gaussian and again use the fact that the conditional expectation $\hat{\mathbf{S}}(\theta) = E(\mathbf{S}_\ell|\mathbf{Y}_\ell)$ has the smallest mean square error. For the general model (5), we obtain

$$
\begin{aligned}
\hat{S}_\ell(\theta) &= f_s G^*(\theta)\Big(G(\theta)f_s G^*(\theta) + P_n I_N \Big)^{-1} \mathbf{Y}_\ell \\
&= \Big(G^*(\theta)G(\theta) + P_n f_s^{-1} \Big)^{-1} G^*(\theta)\mathbf{Y}_\ell,
\end{aligned}
\tag{16}
$$

32

using a standard matrix identity (see, for example, Jazwinski, 1970). The estimator involves computing the delayed quantity $A_j(\theta)Y_{j\ell}$ on each sensor and then adjusting by multiplying by the adjustment matrix involving the spectral matrices of the signal and noise. The mean square covariance matrix of the estimator is given by

$$
\begin{aligned}
\Sigma(\theta) &= f_s - f_s G^*(\theta)\Big(G(\theta)f_s G^*(\theta) + P_n I_N\Big)^{-1} G(\theta)f_s \\
&= P_n\Big(G^*(\theta)G(\theta) + P_n f_s^{-1}\Big)^{-1},
\end{aligned} \tag{17}
$$

using another identity from Jazswinski (1970). We note that for $A_j(\theta)$ as defined in (3) and (4), we have the simplification

$$
G^*(\theta)G(\theta) = I_N, \tag{18}
$$

so that the multilplying matrices in (16) and (17) do not depend on θ and we may write

$$
\hat{\mathbf{S}}_\ell(\theta) = CG^*\mathbf{Y}_\ell \tag{19}
$$

and

$$
\Sigma = P_n C, \tag{20}
$$

where

$$
C = \Big(I_N + P_n f_s^{-1}\Big)^{-1}, \tag{21}
$$

for use in later equations. We notice that the optimal estimator is no longer the beam, but is essentially a weighted beam of the form

$$
\hat{S}_{jl}(\theta) = \sum_{k=1}^{N} c_{jk}\exp\{2\pi i r'_k\theta\}Y_{kl} \tag{22}
$$

with weights proportional to the elements of C defined by (21).

3. Maximum Likelihood Estimation

In the stochastic signal case, we regard the wavenumber vector $\theta = (\theta_1, \theta_2)'$ and the nonlinear functions velocity and azimuth, say

$$
\begin{aligned}
c &= \frac{\nu}{\sqrt{\theta_1^2 + \theta_2^2}} \\
&= \frac{\nu}{\|\theta\|}
\end{aligned} \tag{23}
$$

and

$$
\alpha = \tan^{-1}\big(\theta_2/\theta_1\big) \tag{24}
$$

33

as the parameters to be estimated. The log likelihood function is of the form

$$\log L(\theta) = -L \log |f_y(\theta)| - \sum_{\ell=1}^{L} \mathbf{Y}_\ell^* [f_y(\theta)]^{-1} \mathbf{Y}_\ell, \qquad (25)$$

where the form taken by the spectral density matrix of the data can be either (8) or (12) depending on whether we have the perfect or general correlation models. Suppose, for the moment, that we only want estimators for the velocity and azimuth. Large sample likelihood theory implies that, for a true value of θ, the distribution of $\hat{\theta}$ is approximately normal with mean $\hat{\theta}$ and covariance matrix

$$cov(\hat{\theta}) = \left\{ -E \frac{\partial^2 \log L(\theta)}{\partial \theta \partial \theta'} \right\}^{-1} \qquad (26)$$

Having done this, note that the velocity and azimuth are nonlinear functions, say $\mathbf{h}(\theta) = (c, \alpha)' = (h_1(\theta), h_2(\theta))'$ and the delta method implies that the function is approximately normal with mean $\mathbf{h}(\theta_0)$ and

$$cov(\mathbf{h}(\theta) = \left(\frac{\partial \mathbf{h}}{\partial \theta} \right) cov(\hat{\theta}) \left(\frac{\partial \mathbf{h}}{\partial \theta} \right)' \qquad (27)$$

For the velocity and azimuth functions, note that

$$\frac{\partial \mathbf{h}}{\partial \theta} = \frac{1}{\|\theta\|^3} \begin{pmatrix} -\nu\theta_1 & -\nu\theta_2 \\ \|\theta\|\theta_2 & -\|\theta\|\theta_1 \end{pmatrix} \qquad (28)$$

The following sections discuss maximum likelihood estimation and derive the limiting distribution of the maximum likelihood estimators for velocity and azimuth. We also derive the likelihood ratio detectors for the signal and its distribution for the perfectly correlated case.

3.1 Maximum Likelihood: The Perfectly Correlated Signal

For the perfectly correlated case, with covariance matrix (11), we may write the log likelihood function (25) as

$$\log L(\theta) = -L \log \frac{P_s}{(N+r)} - \frac{1}{P_n} \sum_{\ell=1}^{L} \mathbf{Y}_\ell^* \mathbf{Y}_\ell + \frac{1}{P_n} \frac{\sum_{\ell=1}^{L} |\mathbf{g}^*(\theta)\mathbf{Y}_\ell|^2}{N+r}. \qquad (29)$$

This is seen to be a monotone function of the beam power which will be proportional to

$$B(\theta) = \sum_{\ell=1}^{L} |\mathbf{g}^*(\theta)\mathbf{Y}_\ell|^2. \qquad (30)$$

34

Hence, to maximize the log likelihood, it will be sufficient to maximize the beam power (30) over θ.

Suppose that we look for the liklihood ratio criterion for testing the presence or absence of the signal S_ℓ. Then, for $S_\ell = 0$, we will obtain a test statistic that is a monotone function of the beam power in (30). For any θ, under the hypothesis $P_s = 0$, the distribution of $B(\theta)$ is proportional to a chi-squared distribution with $2L$ degrees of freedom, i.e.

$$\frac{2B(\theta)}{NP_n} \sim \chi^2(2L). \tag{31}$$

Under the alternative hypthesis, assuming the wavenumber vector is evaluated at the correct θ, we have

$$\frac{2B(\theta)}{NP_n} \sim \left(1 + N\frac{P_s}{P_n}\right)\chi^2(2L). \tag{32}$$

If θ_0 is the model value and we use the beam at θ, the distribution of the test statistic is

$$\frac{2B(\theta)}{NP_n} \sim \left(1 + d(\theta, \theta_0)\frac{P_s}{P_n}\right), \tag{33}$$

where

$$d(\theta, \theta_0) = N^{-1} \sum_{j=1}^{N} \sum_{k=1}^{N} \cos[2\pi(\mathbf{r}_j - \mathbf{r}_k)'(\theta - \theta_0)] \tag{34}$$

and the detection probability is a function of the offset between θ and θ_0.

The uncertainty of the maximum likelihood estimators for velocity and azimuth are evaluated by using (26)-(28) in conjunction with the log likelihood (29) and we note that the covariance matrix of θ simplifies, since

$$\frac{\partial^2 \log L(\theta)}{\partial\theta\partial\theta'} = -\frac{(2\pi)^2}{P_n(N+r)} \sum_{j,k} \sum_{\ell=1}^{L} \exp\{2\pi i(\mathbf{r}_j - \mathbf{r}_k)'\theta\} Y_{j\ell} Y_{k\ell}^*(\mathbf{r}_j - \mathbf{r}_k)(\mathbf{r}_j - \mathbf{r}_k)'.$$

Hence,

$$-E\left\{\frac{\partial^2 \log L(\theta)}{\partial\theta\partial\theta'}\right\} = (2\pi)^2 \frac{L}{(N+r)} \frac{P_s}{P_n} \sum_{j,k} (\mathbf{r}_j\mathbf{r}_j' - \mathbf{r}_j\mathbf{r}_k' - \mathbf{r}_k\mathbf{r}_j' + \mathbf{r}_k\mathbf{r}_k')$$

$$= \frac{2(2\pi)^2 N^2 L}{r(N+r)} R, \tag{35}$$

where

$$R = \frac{1}{N} \sum_{j=1}^{N} (\mathbf{r}_j - \bar{\mathbf{r}})(\mathbf{r}_j - \bar{\mathbf{r}})' \tag{36}$$

35

is the sample covariance matrix of the array of the array coordinates. It follows that $\hat{\theta}$ will be approximately normal with mean zero and approximate covariance matrix

$$cov(\hat{\theta}) \approx \frac{1}{2(2\pi)^2} \frac{1}{L} \frac{r}{N} \left(1 + \frac{r}{N}\right) R^{-1} \tag{37}$$

where r is the inverse of the signal-to-noise ratio (13). Then, defining the vectors $\theta = (\theta_1, \theta_2)'$ and $\tilde{\theta} = (\theta_2, -\theta_1)'$, we obtain the variance estimators for

$$var\ \hat{c} \approx \frac{1}{2(2\pi)^2} \frac{r}{N} \left(1 + \frac{r}{N}\right) \frac{\nu^2}{\|\theta\|^6} \frac{\theta' R^{-1} \theta}{L} \tag{38}$$

and

$$var\ \hat{\alpha} \approx \frac{1}{2(2\pi)^2} \frac{r}{N} \left(1 + \frac{r}{N}\right) \frac{1}{\|\theta\|^4} \frac{\tilde{\theta}' R^{-1} \tilde{\theta}}{L}. \tag{39}$$

Evaluating the above equations at $\hat{\theta}$ will produce consistent estimators for the variances.

3.1 Maximum Likelihood: The General Correlated Signal

For the signal with a general correlation structure, as in (1), the log likelihood has the covariance structure given by (7) and we write (24) in the form

$$\log L(\theta) \propto -L \log |f_s| - \log |I_N + P_n f_s^{-1}|$$
$$- \frac{1}{P_n} \sum_\ell Y_\ell^* Y_\ell + \frac{1}{P_n} \sum_l Y_\ell^* G(\theta) \left(I_N + P_n f_s^{-1}\right)^{-1} G^*(\theta) Y_\ell. \tag{40}$$

Then, noting that the Hermitian form contains the matrix C in (21), we may write the likelihood ratio detector in the form

$$\tilde{B}(\theta) = \frac{1}{P_n} \sum_{\ell=1}^{L} \hat{S}_\ell^*(\theta) C^{-1} \hat{S}_\ell(\theta) \tag{41}$$

using (18). The detector does not seem to have a tractable distribution and it may be better to compare $2 \log L(\hat{\theta}) - 2 \log L$ with a χ_2^2 distribution where $\log L$ denotes the value of (40) evaluated at $f_s = 0$.

We may derive variance formulae using an argument similar to that for the perfectly correlated case. First, note that

$$\frac{\partial^2 \log L(\theta)}{\partial \theta \partial \theta'} = \frac{\partial^2}{\partial \theta \partial \theta'} \left\{ \frac{1}{P_n} \sum_{\ell=1}^{L} Y_\ell^* G(\theta) C G(\theta) Y_\ell \right\}$$
$$= \frac{\partial^2}{\partial \theta \partial \theta'} \left\{ \frac{1}{P_n} \sum_{j,k} \sum_\ell Y_{j\ell}^* Y_{k\ell} c_{jk} \exp\{-2\pi i (r_j - r_k)' \theta\} \right\}$$
$$= -(2\pi)^2 \frac{1}{P_n} \sum_{j,k} \sum_\ell c_{jk} Y_{j\ell}^* Y_{k\ell} (r_j - r_k)(r_j - r_k)' \exp\{-2\pi i (r_j - r_k)' \theta\}.$$

36

Taking expectations, we obtain

$$-E\left\{\frac{\partial^2 \log L(\theta)}{\partial\theta\partial\theta'}\right\} = (2\pi)^2 \frac{L}{P_n} \sum_{j,k} c_{jk} f_{kj}^s (\mathbf{r}_j - \mathbf{r}_k)(\mathbf{r}_j - \mathbf{r}_k)'$$

$$= (2\pi)^2 \frac{L}{P_n} D, \tag{42}$$

where f_{jk}^s denotes the jk^{th} element of the signal spectral matrix and

$$D = \sum_{j,k} c_{jk} f_{kj}^s (\mathbf{r}_j - \mathbf{r}_k)(\mathbf{r}_j - \mathbf{r}_k).' \tag{43}$$

In this case we will have $\hat\theta$ distributed approximately as a normal random variable with mean θ_0 and covariance matrix

$$cov\ \hat\theta \approx \frac{1}{(2\pi)^2} \frac{P_n}{L} D \tag{44}$$

leading to estimated variances for the velocity and azimuth of the form

$$var\ \hat c \approx \frac{1}{(2\pi)^2} P_n \frac{\nu^2}{\|\theta\|^6} \frac{\theta' D^{-1} \theta}{L} \tag{45}$$

and

$$var\ \hat\alpha \approx \frac{1}{(2\pi)^2} P_n \frac{1}{\|\theta\|^4} \frac{\tilde\theta' D^{-1} \tilde\theta}{L} \tag{46}$$

REFERENCES

Brillinger, D.R. (1985). A maximum likelihood approach to frequency-wavenumber analysis. *IEEE Trans. on Acoustics, Speech and Signal Processing* **33** 1076-1085.

Capon, J. (1969). High resolution frequency wavenumber spectrum analysis. *Proc. IEEE* **57** 1408-1418.

Harris, D. B. (1990) Comparison of the direction estimation performance of high-frequency seismic arrays and three- component stations. *Bull. Seismolog. Soc. Amer.* **80** 1951-1968.

Hinich, M.J. (1981). Frequency-wavenumber array processing. *J. Acoust. Soc. Amer.* **69** 732-737.

Hinich, M.J. and P. Shaman (1972). Parameter estimation for an R-dimensional plane wave observed with additive independent Gaussian errors. *Ann. Math. Statist.* **43** 153-169.

Jazwinski, A.H. (1970). *Stochastic Processes and Filtering Theory.* Appendix 7B, pp. 261-262. New York: Academic Press

Shumway, R.H. (1983). Replicated time series regression: An approach to signal estimation and detection. In Brillinger, Krishnaiah ed. *Handbook of Statistics, Vol. 3, Time Series in the Frequency Domain* Amsterdam: North Holland.

Wu, J. S-H (1982). Asymptotic properties of nonlinear least squares estimators in a replicated time series model. (1982). Ph.D. Dissertation, The George Washington University, Washington, D.C.

APPENDIX: Variance of Beamforming Estimator Under Signal Decorrelation

For the original estimated wavenumber in the decorrelated signal case, we have

$$\hat{\theta} \sim AN\left(\theta_0, \frac{1}{(2\pi)^2}P_n D^{-1}\right)$$

where

$$D = \sum_{i,j} c_{ij} f_{ji}^s (\mathbf{r}_i - \mathbf{r}_j)(\mathbf{r}_i - \mathbf{r}_j)'$$

with

$$C = (I_N + P_n f_s^{-1})^{-1}$$

For the maximizer of the beam power, say

$$Q(\theta) = \sum_{\ell=1}^{L} |\mathbf{g}^*(\theta)\mathbf{Y}_\ell|^2,$$

say $\hat{\theta}_B$, we have

$$\hat{\theta}_B \sim AN\left(\theta_0, \frac{1}{(2\pi)^2}V^{-1}WV^{-1}\right),$$

where

$$W = \sum_{i,j,i',j'} (\mathbf{r}_i - \mathbf{r}_j)(\mathbf{r}_{i'} - \mathbf{r}_{j'})' f_{ii'}^s f_{j'j}^s$$

$$+ \sum_{i,i',j}(\mathbf{r}_i - \mathbf{r}_j)(\mathbf{r}_{i'} - \mathbf{r}_j)' f_{ii'}^s P_n + \sum_{j,j',i}(\mathbf{r}_i - \mathbf{r}_j)(\mathbf{r}_i - \mathbf{r}_{j'})' f_{j'j}^s P_n$$

$$+ \sum_{i,j}(\mathbf{r}_i - \mathbf{r}_j)(\mathbf{r}_i - \mathbf{r}_j)' P_n^2$$

and

$$V = \sum_{i,j}(\mathbf{r}_i - \mathbf{r}_j)(\mathbf{r}_i - \mathbf{r}_j)' f_{ij}^s$$

We get

$$var\ \hat{\alpha} \approx \frac{1}{(2\pi)^2}P_n \frac{1}{\|\theta\|^4} \frac{\tilde{\theta}' D^{-1}\tilde{\theta}}{L}$$

and

$$var\ \hat{\alpha}_B \approx \frac{1}{(2\pi)^2}\frac{1}{\|\theta\|^4} \frac{\tilde{\theta}' V^{-1}WV^{-1}\tilde{\theta}}{L}$$

```
function y = fsnewth(c,T,B,tw,sni,ax,deg,dc)

% function y = snewth(c,T,B,tw,sni,xx)
% standard error in degrees of optimum beamed estimate
& of signal with imperfect correlation
% fs returns matrix of coherences between sensors
% c: velocity km/sec, T: signal period seconds,
% k equals 1/wavelength, not 2*pi/wavelength
% ax is N rows by 2 columns, x and y coordinates in km
% B: bandwidth, tw: time window, sni: amplitude S/N on each element
% N: number of sensors in array
% az is 0 to the north and increases clockwise,
% deg: 1/2 delta azimuth e.g. 5 degrees
% dc: delta velocity in km/sec, e.g. for infrasound 0.015
% d is D/Ps and is the coherence-weighted array covariance matrix corresponding
% to R; Ps is the signal power spectrum

%
%y=(180/pi)*(1/(2*pi))*((c*T)/sqrt(xx))*sqrt((1/(2*B*tw))*(1/(N*sni^2))*(1+(1/(N*sni^2))));


N=size(ax,1);
fsm=fs(c,T,az,ax,deg,dc);
cc=inv(eye(N)+(1/sni^2)*(inv(fsm))):
d=zeros(2);
for id=1:2;
for jd=1:2;
 for j=1:N;
 for k=1:N;
 d(id,jd)=d(id,jd)+cc(j,k)*fsm(k,j)*(ax(j,id)-ax(k,id))*(ax(j,jd)-ax(k,jd));
 end
 end
end
end


ko=1/(c*T); kx=ko*sin(pi/2-az); ky=ko*cos(pi/2-az);
theta=[ky -kx]';
kidk=theta'*inv(d)*theta;
y=(180/pi)*(1/(2*pi))*(1/sqrt(sni^2*B*tw))*(1/ko^2)*sqrt(kidk);
```

```
function y = bfsnewth(c,T,B,tw,sni,ax,az,deg,dc)

% standard error in degrees of beamed estimate
& of signal with imperfect correlation
% fs returns matrix of coherences between sensors
% c: velocity km/sec, T: signal period seconds,
% k equals 1/wavelength, not 2*pi/wavelength
% ax is N rows by 2 columns, x and y coordinates in km
% B: bandwidth, tw: time window, sni: *amplitude* S/N on each element
%    (in text snr is *power* S/N, therefore sni^2 in formulas below)
% N: number of sensors in array
% az is 0 to the north and increases clockwise,
% deg: 1/2 delta azimuth e.g. 5 degrees
% dc: delta velocity in km/sec, e.g. for infrasound 0.015
% v is V/(Pn*sni^2) is the coherence-weighted array covariance matrix
% w is W/Pn**2, note in final formula sni^4 instead of sni^2 in
%  optimum formula "because" of sni^4 in w

% Note for perfect correlation:
% y=(180/pi)*(1/(2*pi))*sqrt((1/(2*B*tw))*(1/(N*sni^2))
% *(1+(1/N*sni^2))))*((c*T)/sqrt(xx));


N=size(ax,1);
fsm=fs(c,T,az,ax,deg,dc);
v=zeros(2);
w=zeros(2);
for id=1:2;
for jd=1:2;
 for i=1:N;
 for j=1:N;
v(id,jd)=v(id,jd)+fsm(i,j)*(ax(i,id)*(ax(j,id)-ax(j,jd)));
 end
 end
end
end

for id=1:2;
for jd=1:2;
 for i=1:N;
 for j=1:N;
w(id,jd)=w(id,jd)+ (ax(i,id)-ax(j,id)*(ax(i,jd)-ax(j,jd));
 end
 end
end
end
```

```
for id=1:2;
for jd=1:2;
 for i=1:N;
 for j=1:N;
 for jp=1:N;
 w(id,jd)=w(id,jd)+fsm(jp,j)*sni^2*(ax(i,id)-ax(j,id))*(ax(i,jd)-ax(jp,jd));
 end
 end
 end
end
end

for id=1:2;
for jd=1:2;
 for i=1:N;
 for j=1:N;
 for ip=1:N;
 w(id,jd)=w(id,jd)+fsm(i,ip)*sni^2*(ax(i,id)-ax(j,id))*(ax(ip,jd)-ax(j,jd));
 end
 end
 end
end
end

for id=1:2;
for jd=1:2;
 for i=1:N;
 for j=1:N;
 for ip=1:N;
 for jp=1:N;
 w(id,jd)=w(id,jd)+fsm(i,ip)*sni^2*fsm(jp,j)*sni^2*(ax(i,id)-ax(j,id))*(ax(ip,jd)-ax(jp,jd));
 end
 end
 end
 end
end
end

ko=1/(c*T); kx=ko*sin(pi/2-az); ky=ko*cos(pi/2-az);
theta=[ky -kx]';
kidk=theta'*inv(v)*w*inv(v)*theta;
y=(180/pi)*(1/(2*pi))*(1/sqrt(sni^4*B*tw))*(1/ko^2)*sqrt(kidk);
```

```
function fsm=fs(c,T,az,a,deg,dc)

% coherence matrix for array azimuth estimation
% a is array element location x,y matrix
% a is N rows by 2 columns, x and y coordinates in km

% c: velocity km/sec, T: signal period seconds, az: event azimuth
% az is 0 to the north and increases clockwise,
% x1,x2,y1,y2: coordinates of sensors,
% deg: 1/2 delta azimuth e.g. 5 degrees
% dc: delta velocity in km/sec, e.g. for infrasound 0

N=size(a,1);
for i=1:N
 for j=1:N
  x1=a(i,1);x2=a(j,1);y1=a(i,2); y2=a(j,2);
  fsm(i,j)=(gams(c,T,az,x1,x2,y1,y2,deg,dc));
 end
end
```

```matlab
function z = gams(c,T,az,x1,x2,y1,y2,deg,dc)

% function z = gams(c,T,az,x1,x2,y1,y2,deg,dc)
% squared coherence of signal propagating between two stations
% Mack and Flinn Geophysical Journal (1971), 26, p 263, eqn (3)
% c: velocity km/sec, T: signal period seconds, az: event azimuth in radians,
% az is 0 to the north and increases clockwise
% az in radians, e.g. 30 degrees is pi/6 (modified so az in degrees)
% thr is 0 to east and increases counter-clockwise
% x1,x2,y1,y2: coordinates of sensors, deg: 1/2 delta azimuth e.g. 5 degrees
% dc: delta velocity in km/sec, e.g. for infrasound 0.015

az=(az/90)*pi/2;
ko=1/(c*T);
dth = pi*deg/180;
% dth is 1/2 delta azimuth in radians

dk = 1/(c*T) -1/((c+dc)*T);

thr=atan2(y2-y1,x2-x1);
thd=(pi/2 - az) - thr;
% thd is angle from r to k, positive counter-clockwise

r=sqrt((y2-y1)^2+(x2-x1)^2);
y=r*cos(thd);x=r*sin(thd);

if x == 0; x=eps; end;
if y == 0; y=eps; end;

arg1=2*pi*ko*x*sin(dth); arg2=2*pi*dk*y;


zr=(sin(arg1)/arg1)*(sin(arg2)/arg2);
z=zr^2
```

DISTRIBUTION

California Institute of Technology
ATTN: Prof. Thomas Ahrens
Seismological Laboratory, 252-21
Pasadena CA 91125

Air Force Research Laboratory/VSBL
ATTN: Dr. Robert Raistrick
29 Randolph Rd.
Hanscom AFB MA 01731-3010

OATSD(NCB)/NT
ATTN: Mr. Patrick Wakefield
1515 Wilson Blvd., Suite 720
Arlington VA 22209

Pennsylvania State University
ATTN: Prof. S. Alexander & Prof. C. Langston
Department of Geosciences
537 Deike Building
University Park PA 16802

University of Colorado
ATTN: Prof. C. Archambeau, Prof. D. Harvey,
  Dr. Anatoli Levshin, & Prof. M. Ritzwoller
Department of Physics/JSPC
3100 Marine Street
Boulder CO 80309-0583

Cornell University
ATTN: Prof. M. Barazangi
Institute for the Study of the Continents
Department of Geological Sciences
3126 SNEE Hall
Ithaca NY 14853

State University of New York, Binghamton
ATTN: Prof. F.T. Wu
Department of Geological Sciences
Binghamton NY 13901

ENSCO, Inc./APA Division
ATTN: Dr. D.R. Baumgardt & Dr. Z. Der
5400 Port Royal Road
Springfield VA 22151-2388

University of Arizona
ATTN: Dr. S. Beck & Prof. T.C. Wallace
Department of Geosciences
Gould Simpson Building
Tuscon AZ 85721

Maxwell Technologies, Inc.
ATTN: Dr. T.J. Bennett & Mr. J. Murphy
Geophysics & Resource Technologies Group
11800 Sunrise Valley Drive, Suite 1212
Reston VA 22091

University of California, San Diego
ATTN: Dr. J. Berger, Dr. L. Burdick,
  Dr. M. Hedlin, Prof. B. Minster,
  Prof. J.A. Orcutt, & Dr. F.L. Vernon
Scripps Institution of Oceanography
Institute of Geophysics and Planetary Physics
9500 Gilman Dr.
La Jolla CA 92093

US Department of Energy
ATTN: Ms. Leslie A. Casey
NNSA/NA-22
1000 Independence Ave., SW
Washington DC 20585-0420

Multimax, Inc.
ATTN: Dr. W. Chan, Dr. I.N. Gupta,
  & Mr. W. Rivers
1441 McCormick Drive
Largo MD 20774

Virginia Polytechnical Institute
ATTN: Dr. M. Chapman
Seismological Observatory
Department of Geological Sciences
4044 Derring Hall
Blacksburg VA 24061-0420

US Department of State
AC/VC
ATTN: Dr. M. Dreicer, Dr. C. Yeaw,
  Dr. W. Leith, & Mr. R. Morrow
2201 C Street, N.W.
Washington DC 20520

University of Connecticut, Storrs
ATTN: Prof. V.F. Cormier
Department of Geology & Geophysics
U-45, Room 207
Storrs CT 06269-2045

DTRA/TDAS
ATTN: Dr. Anton Dainty, Dr. Jay Davis, &
   Dr. R.A. Gustafson
8725 John J. Kingman Rd., MS6201
Ft. Belvoir VA 22060

DTRA/OSTN
ATTN: Dr. C. Gallaway & Dr. R. Goodwin
6801 Telegraph Rd.
Alexandria VA 222310

DTRA/CP
ATTN: Dr. Hopkins
6801 Telegraph Rd.
Alexandria VA 222310

Defense Technical Information Center
8725 John J. Kingman Road, Suite 0944
Ft. Belvoir VA 22060-6218

University of California, San Diego
ATTN: Dr. Catherine de Groot-Hedlin
Institute of Geophysics & Planetary Sciences
8604 La Jolla Shores Drive
San Diego CA 92093

Harvard University
ATTN: Prof. A. Dziewonski
Hoffman Laboratory
Department of Earth, Atmospheric & Planetary
   Sciences
20 Oxford Street
Cambridge MA 02138

Boston College
ATTN: Prof. J. Ebel & Prof. A. Kafka
Department of Geology & Geophysics
Chestnut Hill MA 02167

Mission Research Corporation
ATTN: Dr. M. Fisk & Dr. W. Wortman
8560 Cinderbed Rd., Suite 700
Newington VA 22122

Southern Methodist University
ATTN: Dr. Henry Gray
Department of Statistical Science
P.O. Box 750302
Dallas TX 75275-0302

Pacific Northwest National Laboratories
ATTN: Dr. D.N. Hagedorn
P.O. Box 999, MS K5-12
Richland WA 99352

Lawrence Livermore National Laboratory
ATTN: Dr. J. Zucca
P.O. Box 808, L-205
Livermore CA 94551

MIT ERL E34-404
ATTN: Dr. David Harkrider
42 Carlton St.
Cambridge MA 02142-1324

New Mexico State University
ATTN: Prof. Thomas Hearn & Prof. James Ni
Department of Physics, 3D
Las Cruces NM 88003

California Institute of Technology
ATTN: Dr. Donald Helmberger
Division of Geological & Planetary Sciences
Seismological Laboratory
Pasadena CA 91125

Southern Methodist University
ATTN: Dr. E. Herrin & Dr. B. Stump
Department of Geological Sciences
P.O. Box 750395
Dallas TX 75275-0395

Sandia National Laboratories
ATTN: Mr. Pres Herrington
P.O. Box 5800, MS 0975
Albuquerque NM 87185-0975

St. Louis University
ATTN: Prof. R. Herrmann & Prof. B. Mitchell
Department of Earth & Atmospheric Sciences
3507 Laclede Ave.
St. Louis MO 63103

University of California, Berkeley
ATTN: Prof. L.R. Johnson & Prof. T. McEvilly
Earth Sciences Division
LBNL 90-2106, MS 90-1116
479 McCone Hall
Berkeley CA 94720

Massachusetts Institute of Technology
ATTN: Prof. T.H. Jordan
Department of Earth, Atmospheric, & Planetary
    Sciences
77 Massachusetts Ave., 654-918
Cambridge MA 02139

Massachusetts Institute of Technology
ATTN: Dr. R. LaCross, M-200B
Lincoln Laboratory
P.O. Box 73
Lexington MA 02173-0073

University of Illinois, Urbana-Champaign
ATTN: Prof. F.K. Lamb & Prof. J. Sullivan
Department of Physics
1110 West Green Street
Urbana IL 61801

Oklahoma Geological Survey Observatory
ATTN: Dr. J. Lawson, Chief Geophysicist
Number One Observatory Lane
P.O. Box 8
Leonard OK 74043-0008

University of California, Santa Cruz
ATTN: Dr. T. Lay, Dr. S. Schwartz, & Dr. R. Wu
Institute of Tectonics, Earth Sciences Dept.
A232 Earth & Marine Sciences Building
Santa Cruz CA 95064

US Geological Survey
ATTN: Dr. John Filson
12201 Sunrise Valley Dr., MS-905
Reston VA 22092

Weston Geophysical Corp.
ATTN: Mr. James Lewkowicz
57 Bedford St., Ste 102
Lexington MA 02420

Georgia Institute of Technology
ATTN: Prof. L. Long
School of Geophysical Sciences
Atlanta GA 30332

Southern Methodist University
ATTN: Dr. G. McCartor
Department of Physics
P.O. Box 750175
Dallas TX 75275-0175

US Geological Survey
ATTN: Dr. A. McGarr
National Earthquake Center
345 Middlefield Rd., MS-977
Menlo Park CA 94025

Office of the Secretary of Defense
DDR&E
Washington DC 20330

Yale University
ATTN: Prof. J. Park
Department of Geology & Geophysics
P.O. Box 208109
New Haven CT 06520-8109

University of Cambridge
ATTN: Prof. Keith Priestly
Bullard Lab, Department of Earth Sciences
Madingley Rise, Madingley Road
Cambridge CB3 OEZ
UNITED KINGDOM

BBN Systems & Technologies
ATTN: Dr. J.J. Pulli
1300 N. 17th St., Suite 1200
Arlington VA 22209

DTR Associates/Weston Geophysical
ATTN: Dr. Delaine Reiter
325 West Main Street
Northborough MA 01532

Columbia University
ATTN: Prof. P. Richards & Dr. J. Xie
Lamont-Doherty Earth Observatory
61 Route 9W
Palisades NY 10964

Woodward-Clyde Federal Services
ATTN: Dr. C.K. Saikia
566 El Dorado Street, Suite 100
Pasadena CA 91101-2560

University of Southern California, Los Angeles
ATTN: Prof. C.G. Sammis
Center for Earth Sciences
University Park
Los Angeles CA 90089

Secretary of the Air Force
(SAFRD)
Washington DC 20330

University of California, Davis
ATTN: Dr. R. Shumway
Division of Statistics
1 Shields Ave.
Davis CA 95616-8671

AFOSR/NL
110 Duncan Avenue, Suite B115
Bolling AFB
Washington DC 20332-0001

Los Alamos National Laboratory
ATTN: Dr. H. Patton, Dr. S.R. Taylor,
    Dr. C.L. Edwards, Dr. D.C. Pearson, &
    Dr. Scott Phillips
P.O. Box 1663, MS D408
Los Alamos NM 87545

Massachusetts Institute of Technology
ATTN: Prof. M.N. Toksoz
Earth Resources Lab, 34-440
42 Carleton Street
Cambridge MA 02142

WINPACC/CA/FO
ATTN: Dr. L. Turnbull
New Headquarters Bldg., Room 4W03
Washington DC 20505

National Science Foundation
ATTN: Dr. Daniel Weill
Division of Earth Sciences, EAR-785
4201 Wilson Blvd., Room 785
Arlington VA 22230

NTNF/NORSAR
ATTN: Dr. Svein Mykkeltveit
Granaveien 33
P.O. Box 51
N-2007 Kjeller
NORWAY

Australian Geological Survey Organization
ATTN: Dr. David Jepsen
Cnr. Jerragomerra Ave. & Nindmarsh Dr.
Canberra, ACT 2609
AUSTRALIA

Atomic Weapons Establishment
ATTN: Dr. P. Marshall, Dr. David Bowers, &
    Dr. Alan Douglas
Blacknest, Brimpton
Reading FG7 4RS
UNITED KINGDOM

University of Bergen
ATTN: Prof. Eystein Husebye
Institute for Solid Earth Physics, IFJ
Allegaten 41
N-5007, Bergen
NORWAY

AFTAC/CA(STINFO)/TT/TTD/TTE/TTR
1030 South Highway A1A
Patrick AFB FL 32925-3002

(This page intentionally left blank.)